Geological Magazine

www.cambridge.org/geo

Early Permian subduction-related transtension in the Turpan Basin, East Tianshan (NW China): implications for accretionary tectonics of the southern Altaids

Qigui Mao[1,2], Wenjiao Xiao[3,4], Brian F. Windley[5], Minjie Yu[1], Min Sun[6], Songjian Ao[4,7] and Ji'en Zhang[4,7]

[1]Beijing Institute of Geology for Mineral Resources, Beijing 100012, China; [2]Deep Exploration Technic Center for Non-ferrous Mines, Beijing 10012, China; [3]Xinjiang Research Center for Mineral Resources, Xinjiang Institute of Ecology and Geography, Chinese Academy of Sciences, Urumqi 830011, China; [4]College of Earth and Planetary Sciences, University of Chinese Academy of Sciences, Beijing 100049, China; [5]Department of Geology, University of Leicester, Leicester LE1 7RH, UK; [6]Department of Earth Sciences, University of Hong Kong, Hong Kong, China and [7]State Key Laboratory of Lithospheric Evolution, Institute of Geology and Geophysics, Chinese Academy of Sciences, Beijing 100029, China

Original Article

Cite this article: Mao Q, Xiao W, Windley BF, Yu M, Sun M, Ao S, and Zhang J (2021) Early Permian subduction-related transtension in the Turpan Basin, East Tianshan (NW China): implications for accretionary tectonics of the southern Altaids. *Geological Magazine* **158**: 175–198. https://doi.org/10.1017/S0016756819001006

Received: 23 July 2018
Revised: 12 July 2019
Accepted: 18 July 2019
First published online: 14 November 2019

Keywords:
volcanic rocks; early Permian; A-type granite; transtension; East Tianshan

Author for correspondence:
Wenjiao Xiao, Email: wj-xiao@mail.iggcas.ac.cn

Abstract

The interaction of the Palaeo-Pacific and Palaeo-Asian Oceans is an enigmatic issue as their temporal and spatial features are controversial. To address this issue, we present a systematic study of large volumes of early Permian volcanic rocks and intrusions developed in the East Tianshan. The represented samples of basaltic andesites and rhyolites yield zircon crystallization ages of 285.1 ± 5.9 Ma and 275.3 ± 1.8 Ma, respectively. The basalts have normal mid-ocean ridge basalt (N-MORB) and arc-related geochemical signatures with high TiO_2 contents, negative Rb, Th, U, Nb and Ta anomalies and positive Eu anomalies. Basaltic andesites and andesites have arc-related geochemical characteristics with moderate TiO_2 contents and relatively negative Nb, Ta and Ti anomalies, together with slightly negative to positive Eu anomalies. The rhyolites show an affinity with A_2-type granite with high SiO_2, $K_2O + Na_2O$, Fe/Mg, Ga, Zr, Nb, Y, HFSE, REE and Y/Nb levels (>1.2). These geochemical data suggest that the rocks formed in a supra-subduction zone. The presence of high $\epsilon_{Nd}(t)$ values of +4.6 to +8.2 and low $(^{87}Sr/^{86}Sr)_i$ (0.70342–0.70591) values indicates that the volcanic rocks originated from a depleted mantle. We propose that oblique subduction with slabs breaking off gave rise to transtension and to the emplacement of large volumes of mantle-derived melts in the early Permian in the East Tianshan, serving as an important record of the subduction zone of the Palaeo-Pacific Ocean.

1. Introduction

The Palaeozoic evolution of the Palaeo-Pacific Ocean is an enigmatic issue as its temporal and spatial features are controversial. Some researchers believe that the Pacific Ocean did not operate in the late Palaeozoic in central Asia and only affected NE Asia in the Early Mesozoic, while others have proposed that the Palaeo-Pacific Ocean may have already operated in the Palaeozoic or even earlier (Xiao *et al.* 2010, 2015).

As part of the Palaeo-Pacific Ocean, the Palaeo-Asian Ocean was consumed to form the Altaids (or the Central Asian Orogenic Belt, mainly developed from ~1.0 Ga to 250 Ma), one of the most important sites of juvenile crustal growth (Şengör *et al.* 1993; Şengör & Natal'in, 1996; Xiao *et al.* 2004, 2010, 2015, 2018; Windley *et al.* 2007; Domeier & Torsvik, 2014) (Fig. 1). Therefore, the Altaids serve as an appropriate natural case for determining the systematic anatomy of the Palaeozoic evolution of the Palaeo-Pacific Ocean.

Over decades of study, a consensus has gradually been reached that the Altaids were formed through the successive lateral accretion of small continental blocks, arcs and accretionary complexes (Coleman, 1989; Şengör *et al.* 1993; Dobretsov *et al.* 1995; Şengör & Natal'in, 1996; Ma *et al.* 1997; Gao *et al.* 1998; Buchan *et al.* 2002; Bazhenov *et al.* 2003; Li, 2004; Xiao *et al.* 2004, 2008*b*, 2010; JY Li *et al.* 2006*a*; Windley *et al.* 2007; Shi *et al.* 2010), and through the emplacement of immense volumes of magma in a lateral accretionary, post-collision and/or intraplate extensional setting in the late Palaeozoic and early Mesozoic (Han *et al.* 1997, 1998, 2004; F Chen *et al.* 2000; Jahn *et al.* 2000; Wu *et al.* 2000, 2002; Jahn, 2004; ZH Chen et al. 2006; Windley *et al.* 2007; Yuan *et al.* 2007; Mao *et al.* 2014*c*). To date, the architecture and style of orogenic collages is controversial, and there are two general classes of models. One model suggests that the Altaids formed through a prolonged and steady period of subduction–accretion, followed by the oroclinal bending of a single, long-lived giant magmatic arc complex

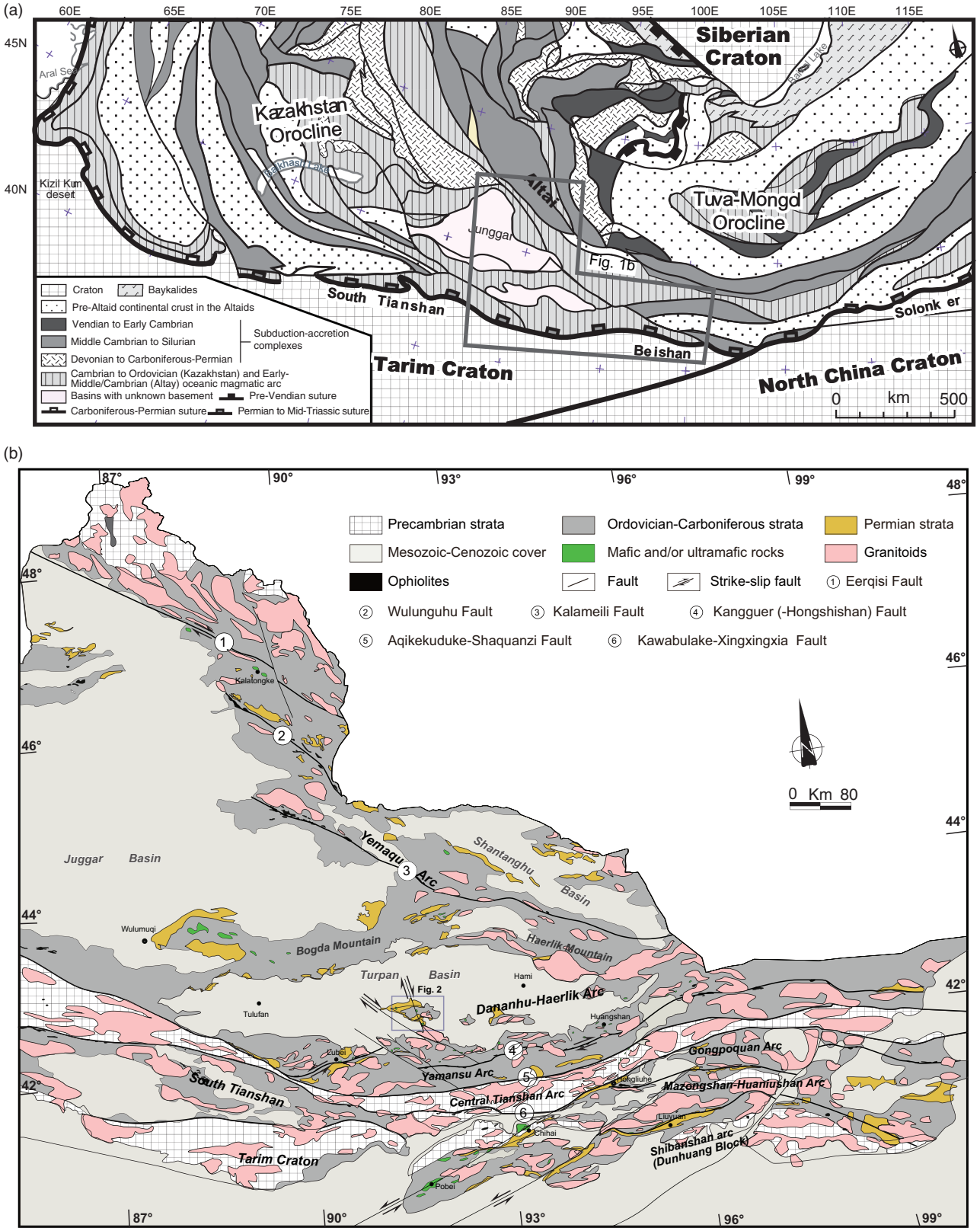

Fig. 1. (a) Schematic tectonic map of central Asia and adjacent regions (Şengör *et al.* 1993; Xiao *et al.* 2015). (b) Schematic geological map of Eastern Tianshan (modified after XBGMR, 1993, and Xiao *et al*. 2004, 2010) showing the locations of the Permian volcanic rocks within the desert of the Turpan Basin. Major faults separate southern Tianshan, central Tianshan, the Yamansu Arc and the Dananhu–Haerlik Arc.

https://doi.org/10.1017/S0016756819001006 Published online by Cambridge University Press

or continental sliver (Şengör *et al.* 1993; Şengör & Natal'in, 1996; Yakubchuk *et al.* 2004; Johnston *et al.* 2013; Xiao *et al.* 2018). Conversely, another hypothesis suggests that the Altaids may have grown through the subduction and accretion of multiple oceanic basins accompanied by the development of individual magmatic arc terranes and microcontinents (Coleman, 1989; Dobretsov *et al.* 1995; Ma *et al.* 1997; Buchan *et al.* 2002; Windley *et al.* 2007; Xiao *et al.* 2004, 2008*a*, 2009, 2010, 2015). Geologists agree that the Altaids underwent an important tectonic transition in the Permian, but it is debated whether the Palaeo-Pacific Ocean had closed (Coleman, 1989; Han *et al.* 1998; Li, 2004; Xiao *et al.* 2004, 2006, 2010; Zhou *et al.* 2004; JY Li *et al.* 2006*a*; Wang *et al.* 2006; Qin *et al.* 2011).

The Chinese East Tianshan is the easternmost segment of the Tianshan mountain range in the southern Altaids; it occupies a key position in the Altaids (Fig. 1). In the early Permian, large volumes of volcanic rock and intrusions developed along regional fault belts and/or extensive basins of the East Tianshan (Fig. 1b; Table 4 further below), creating a unique opportunity to study the geological evolution of the southern Altaids. Geologists have conducted systematic studies of Cu–Ni ore-bearing mafic–ultramafic intrusions (Ma *et al.* 1997; Zhu *et al.* 2002; Xiao *et al.* 2004, 2010; Zhou *et al.* 2004; JY Li *et al.* 2006*b*; Mao *et al.* 2006, 2008, 2012, 2014*c*; Zhao *et al.* 2006*a*; Ao et al. 2010; Chen *et al.* 2011; Qin *et al.* 2011), and diverse models have been applied to the Permian geological evolution of the East Tianshan (e.g. the post-collision model (Han *et al.* 1998; Zhou *et al.* 2004; JY Li *et al.* 2006*a*; Wang *et al.* 2006; Qin *et al.* 2011), the oblique subduction model (Xiao *et al.* 2004, 2006, 2010; Mao *et al.* 2008; Ao *et al.* 2010) and the mantle plume model (Pirajno *et al.* 2008; Qin *et al.* 2011; Su *et al.* 2012; Tang *et al.* 2013). The Permian volcano of the East Tianshan has rarely been reported. Permian volcanic rocks in Turpan Basin contains basalt, andesite, dacite and rhyolite, offering new and detailed information on patterns of magmatism in relation to their regional geology and tectonic settings. This paper provides a detailed account of the occurrence and formation of magma relative to the geodynamic development of the southern margin of the Altaids in the Permian.

2. Geological setting

The Chinese East Tianshan is a 300 km wide and 1500 km long orogenic collage (Xiao *et al.* 2004, 2006, 2008*a*, *b*, 2010) consisting of the following tectonic units: South Tianshan, Central Tianshan, the Yamansu Arc and the Dananhu–Haerlik Arc (Fig. 1).

The South Tianshan, located between the Central Tianshan Arc and Tarim Craton (Fig. 1), includes various Silurian–Carboniferous rocks, including turbidites, ophiolites (Silurian – late Carboniferous), cherts, volcaniclastic rocks, mélanges and Devonian – early Carboniferous high-pressure metamorphic rocks (eclogite and blueschist) (Windley *et al.* 1990; Ma *et al.* 1997; Gao *et al.* 1998; Li, 2004; Xiao *et al.* 2004).

The Central Tianshan Arc situated between the Aqikekuduke–Shaquanzi and Kawabulake–Xingxingxia faults (Fig. 1) includes a Precambrian amphibolite facies basement, Palaeozoic plutons and volcanic rocks. The Precambrian basement consists of gneisses, quartz schists, migmatites and marbles dated from 900 to 1900 Ma (Gu *et al.* 1990; Xiu *et al.* 2002; Liu *et al.* 2004; Zhang *et al.* 2004; Hu *et al.* 2006, 2010; Li *et al.* 2009; Shi *et al.* 2010). Palaeozoic arc volcanic rocks, volcanic clastics and intrusions also formed from the Ordovician to early Permian (Li *et al.* 2001; Li, 2004; Zhang *et al.* 2004; Sun *et al.* 2006; Guo *et al.* 2007; Hu *et al.* 2007; Mao *et al.* 2014*a*). The Aqikuduke fault belt is marked by Palaeozoic ophiolites, ductile strike-slip faults and mafic–ultramafic intrusions (Windley *et al.* 1990; Shu *et al.* 1999; Xiao *et al.* 2004, 2008*a*; Wu *et al.* 2005; Mao *et al.* 2006).

The Yamansu Arc comprises Devonian–Carboniferous calc-alkaline andesites, basalts, rhyolites, tuffs and volcaniclastic rocks interbedded with fine-grained clastic rocks and carbonates that have undergone sub-greenschist facies metamorphism, together with granitic intrusions (Ji *et al.* 1994; Yang *et al.* 1996, 1998; Ma *et al.* 1997; Gu *et al.* 1999; Xiao *et al.* 2004).

The Dananhu–Haerlik Ordovician–Carboniferous Island Arc located between the Kalameili and Kangguer faults (Fig. 1b) consists of Ordovician to Permian tholeiites to calc-alkaline mafic–felsic lavas, volcanoclastics, tuffs and clastic sediments (Ma *et al.* 1997; Xiao *et al.* 2004; Hou *et al.* 2005; Tang *et al.* 2006). Abundant arc-related granitic intrusions range in age from the Ordovician to early Permian (Li *et al.* 2004; FW Chen *et al.* 2005; Hou *et al.* 2005; Sun *et al.* 2005; Chao *et al.* 2006; Guo *et al.* 2006; Mao *et al.* 2010). The earlier Permian mafic–ultramafic complex zone is located along the southern margins of the arc and stretches across several hundreds of kilometres (Ma *et al.* 1997; Mao *et al.* 2002; Han *et al.* 2004; Xiao *et al.* 2004; Zhou *et al.* 2004; Qin *et al.* 2011).

Early Permian volcanic rocks occur around the Kalatage and Dananhu Palaeozoic geological inlier in the Turpan Basin (Figs 1b, 2). They are classified as a middle Permian Aerbashayi Formation (XBGMR, 1993; Zhu *et al.* 2002; Mao *et al.* 2014*c*) composed of basalts and basaltic andesites interbedded with minor rhyolites in the lower formation and with tuffs, rhyolites and dacites in the upper formation. The Aerbashayi Formation unconformably covers the upper Carboniferous Qishan Formation or the Ordovician–Silurian Volcanic Arc Group (or the lower Devonian Kaltage Formation) and is unconformably overlain by the upper Permian Kula Formation, the low Jurassic Sangonghe Formation and the Quaternary.

A number of early Permian mafic complexes occur along faults of the Kalatage inlier (Mao, 2014). Adjacent are Ordovician (Devonian)–Jurassic low-grade volcanic rocks, volcaniclastic rocks and clastic sediments (Tang *et al.* 2006; Mao *et al.* 2010, 2014*b*, *c*, 2015). The Ordovician–Silurian Volcanic Group (or lower Devonian Kaltage Formation) consists of calc-alkaline basic–felsic volcanic and volcaniclastic rocks, including basalts, andesites, dacites, rhyolites and volcaniclastic rocks (Qin *et al.* 2001; WQ Li *et al.* 2006; Tang *et al.* 2006; Mao *et al.* 2010, 2014*b*, *c*, 2015). The ages of these rocks are poorly constrained (e.g. the lower Devonian (Qin *et al.* 2001; Tang *et al.* 2006), the Ordovician to Devonian (Mao *et al.* 2010, 2014*b*, 2015; Mao, 2014) or the Ordovician–Silurian (WQ Li *et al.* 2006)). The lower Devonian Dananhu Formation, which unconformably overlies Ordovician–Silurian Arc volcanic sequences, consists of biogenic carbonates, clastic sediments and interbedded volcanic rocks. The Upper Carboniferous (Pennsylvanian) Qishan Formation, unconformably overlying the lower Devonian Dananhu Formation, consists of calc-alkaline basaltic and andesitic volcanic rocks, tuffs and clastic sediments. The lower Permian Aqikebulake Formation (P_1a) consists of basic–felsic volcanic rocks and sediments. The upper Permian Kula Formation consists of clastic sediments, and the Triassic is absent in the area. The lower Jurassic Sangonghe Formation contains black shales, shaly sandstones, sandstones, and coalbeds, which lie unconformably on older strata.

https://doi.org/10.1017/S0016756819001006 Published online by Cambridge University Press

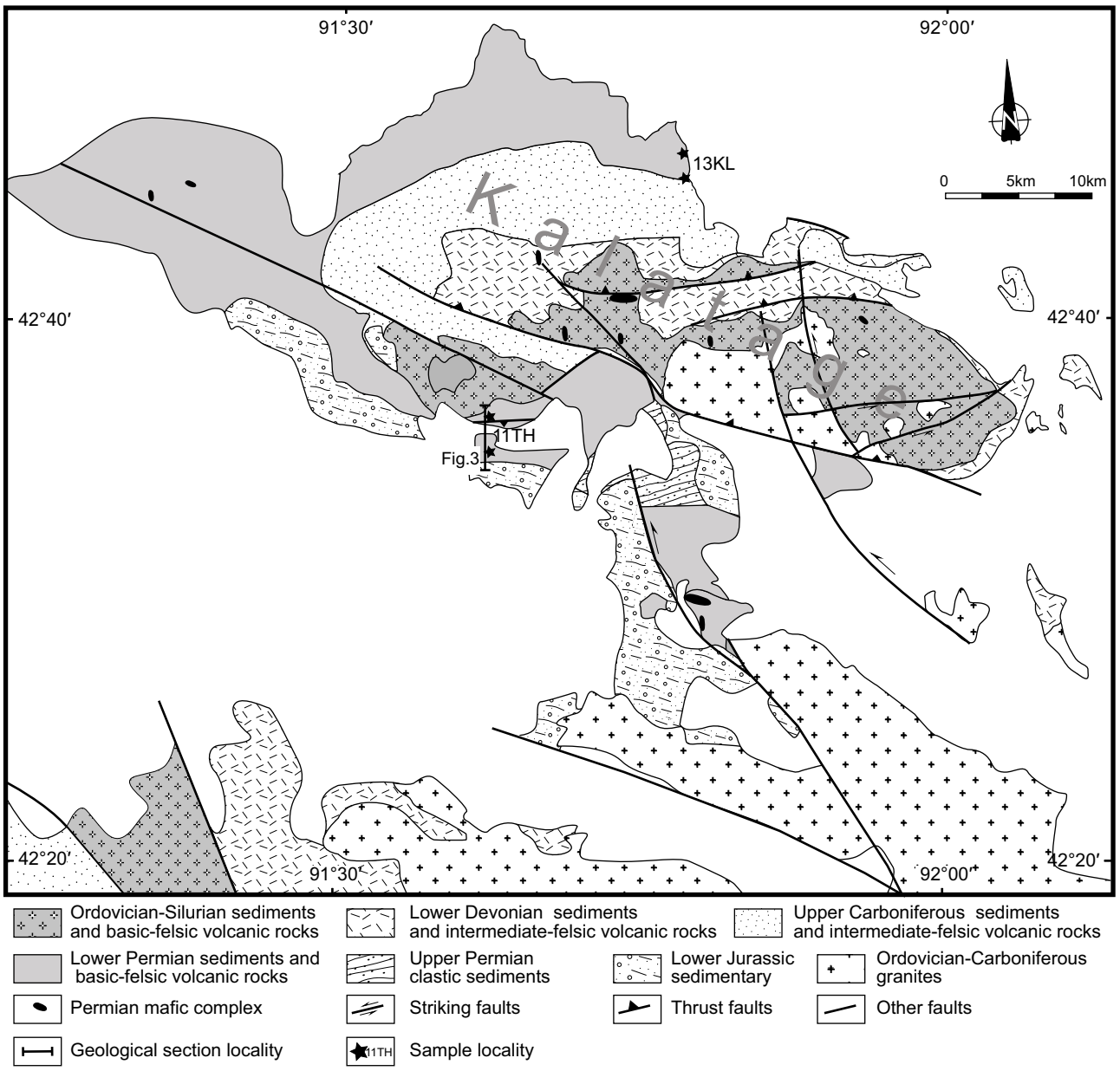

Fig. 2. Geological map of the Kalatage inlier and of an adjacent area of the Turpan Basin (modified after Mao *et al.* 2010, 2014*c*).

3. Sampling and petrography

Figures 1b and 2 show that early Permian volcanic rocks are located in the Turpan Basin and around the Kalatage and Dananhu Palaeozoic geological inlier (Fig. 2). In this study, we mainly research rocks around the Kalatage Palaeozoic geological inlier. Our study reveals a geological section of the southern margins of the Kalatage inlier (Fig. 3). In this section (Fig. 3), early Permian volcanic rocks are mainly composed of clastic sedimentary, amygdaloidal basalts, basalts, basaltic andesites and andesites interbedded with minor rhyolites. From north to south, early Permian volcanic rock formations can be divided into six volcanic–sedimentary sequences. At the bottom are amygdaloidal basaltic andesites and coherent volcaniclastic rocks (11TH01), which unconformably cover the upper Carboniferous Qishan Formation and Ordovician–Silurian volcanic sequences. Next is the sedimentary sequence, which is unconformably covered at the base of volcanic rocks. The third sequence unconformably located on the second sedimentary sequence is composed of sedimentary rocks and interbedded with rhyolites (11TH02 and 13TH01), and a sequence of conglomerates is positioned at the bottom of the sequence. The fourth sequence unconformably covering the third sequence is composed of amygdaloidal basaltic andesites (11TH03 and 13TH03) and coherent volcaniclastic rocks interbedded with a few basalts and rhyolite, which are unconformably covered with a thin layer of rhyolites (11TH04). Thick purple to grey amygdaloidal basalts and volcaniclastic rocks unconformably covering the fourth sequence occur in the upper part of the volcanic formation (11TH05). At the top is a sequence of purple amygdaloidal andesites (11TH06) and volcaniclastic rocks, which are unconformably covered on the fifth sequence and by the low Jurassic Sangonghe Formation. The section suggests a pattern of volcanic eruption varying from basic to intermediate-felsic.

https://doi.org/10.1017/S0016756819001006 Published online by Cambridge University Press

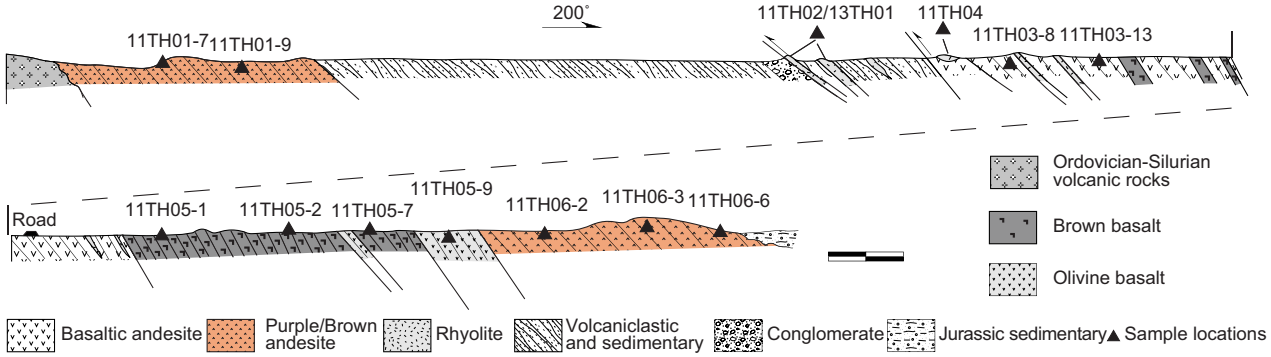

Fig. 3. The geological section for the Permian volcanic rocks in the southern part of the Kalatage inlier.

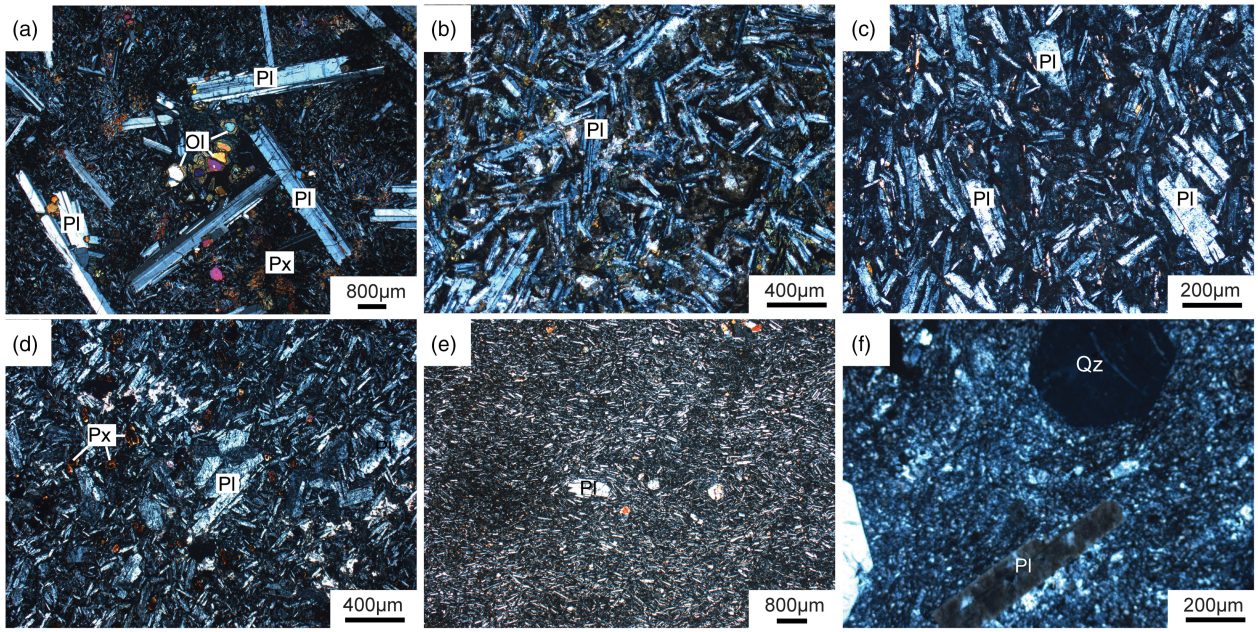

Fig. 4. Microphotographs of volcanic samples around the Kalatage inlier in the Turpan Basin, NW China. (a, b, c) Basalts; (d) basaltic andesites; (e) andesite; (f) rhyolite. Ol – olivine; Px – pyroxene; Pl – plagioclase; Qz – quartz.

To determine the magma composition and age of volcanic rocks in the Turpan Basin, different types of volcanic rocks collected from the Kalatage inlier were analysed for whole rock major, rare earth and trace elements; Sr–Nd isotopic compositions; and basaltic andesites and rhyolite for zircon laser ablation – inductively coupled plasma – mass spectormetry (LA-ICP-MS) U–Pb dating. The sampling locations are shown in geological cross-sections presented in Figures 2 and 3.

Basalts include fine-grained, porphyritic and vesicular types that are greyish-green and brown to purple. The rocks present typical quench textures with abundant phenocrysts (5–40 %) embedded within a fine-grained groundmass (Fig. 4a, b, c). Plagioclase (5–15 %) with a composition of An_{51}–An_{62}, clinopyroxene aggregates and subordinate orthopyroxene (2–20 %) with a composition of Wo_{45}–Wo_{50}, En_{37}–En_{44} and Fs_{6}–Fs_{16}) are of the phenocryst phases along with minor Fe–Ti oxides (1–3 %). The fine-grained groundmass is composed of plagioclase, glass, olivine and Ti-magnetite. Some basalt samples have long plate plagioclase phenocrysts of 0.5–3 cm length and fine-grained olivine phenocrysts (with a composition of $Mg^{\#} = 65–74$ and $Cr^{\#} = 1–38$).

The basaltic andesites and andesites, which are brown to purple, are mainly porphyritic and vesicular and exhibit typical quench textures with abundant phenocrysts (30–50 %) embedded within a fine-grained groundmass (Fig. 4d, e). Plagioclase (30–45 %) and clinopyroxene aggregates (2–5 %) are of the phenocryst phases. The fine-grained groundmass is composed of plagioclase, glass, olivine and Ti-magnetite.

The rhyolites include fine-grained, porphyritic and vesicular types that are grey-white, brown or purple. Rhyolites have a typical porphyritic texture with a few quartz and alkali feldspars as phenocrysts in an aphanitic matrix of the same minerals (Fig. 4f). Quartz phenocrysts are euhedral and 1–3 mm in diameter and are associated with euhedral alkali feldspar phenocrysts of 1–5 mm length. Accessory minerals include zircon, apatite and titanite.

4. Analytical techniques

4.a. Geochronology

Zircon grains were separated using conventional heavy liquid and magnetic techniques. Representative zircon grains were handpicked

https://doi.org/10.1017/S0016756819001006 Published online by Cambridge University Press

under a binocular microscope and mounted in an epoxy resin disc. We used the Sensitive High-Resolution Ion Microprobe (SHRIMP) and LA-ICP-MS zircon U–Pb dating technique to complete the two samples. To identify internal features of the zircons (zoning, structures, alteration, fractures, etc.), cathodoluminescence (CL) images were collected using a Cameca electron microprobe for SHRIMP based at the Chinese Academy of Geological Sciences (Beijing), and LA-ICP-MS dating was conducted at the SEM-EDS-EBSD-CL Laboratory of Peking University (Beijing).

4.a.1. SHRIMP zircon U–Pb dating

The SHRIMP experiments were carried out at the Chinese Academy of Geological Sciences (Beijing). U–Th–Pb isotopic analyses were performed using SHRIMP-II. Further details on the analysis of zircons using SHRIMP are described in Song *et al.* (2002*b*). Inter-element fractionation ion emissions of zircon were corrected relative to RSES reference TEMORA 1 (417 Ma; Black *et al.* 2003). Data reduction was carried out using the Isoplot/Ex v. 2.49 program (Ludwig, 2001).

4.a.2. LA-ICP-MS zircon U–Pb dating

Experiments were carried out at the LA-ICP-MS Laboratory of the University of Science and Technology of China. Uranium, Th and Pb concentrations were calibrated using ^{29}Si as an internal standard and NIST SRM 610 as an external standard. $^{207}Pb/^{206}Pb$ and $^{206}Pb/^{238}U$ ratios were calculated using GLITTER 4.0 (Johnson *et al.* 2008) and were then corrected using Harvard zircon 91500 as an external standard. The $^{207}Pb/^{235}U$ ratio was calculated from the $^{207}Pb/^{206}Pb$ and $^{206}Pb/^{238}U$ values. Common Pb was corrected according to the method proposed by Andersen (2002). Weighted mean U–Pb ages and concordia plots were processed using ISOPLOT 3.0. The procedure is described at length in Xie *et al.* (2008).

4.b. Geochemistry and isotopic studies

Major oxide and trace element experiments were carried out at the analytical laboratory of the Beijing Research Institute of Uranium Geology. Major elements were determined by X-ray fluorescence (XRF) spectrometry with analytical errors of less than 5 %. A loss on ignition (LOI) was determined after igniting the sampled powder at 1000 °C for 1 hour. Trace elements, including rare earth, were identified by ICP techniques, analytical procedures of which are described in Zhou *et al.* (2002). Rb–Sr and Sm–Nd isotopic ratios were measured with a Finnigan MAT262 thermal ionization mass spectrometer (TIMS) housed at the Laboratory for Radiogenic Isotope Geochemistry of the Institute of Geology and Geophysics, Chinese Academy of Sciences, Beijing. Measurements were carried out following the isotope dilution procedures developed by Chen *et al.* (2000) and Zhou *et al.* (2002). A static multi-collection mode was used for the measurements. A traditional cation exchange technique was adopted for chemical separation. Mass fractionation corrections for Sr and Nd isotopic ratios were based on $^{86}Sr/^{88}Sr = 0.1194$ and $^{146}Nd/^{144}Nd = 0.7219$. Repeated measurements of La Jolla Nd standard and NBS987 during the measurement period gave values of $^{143}Nd/^{144}Nd = 0.511861 \pm 9$ (2σ) and $^{87}Sr/^{86}Sr = 0.710254 \pm 10$ (2σ), respectively. Total procedural blanks for Sr and Nd are valued at ~10^{-9} and ~10^{-11} g, respectively.

5. Results

Two new zircon U–Pb dates for andesite and rhyolite are presented in Figure 4 and Table 1, respectively. Major and trace elements and Sm–Nd and Rb–Sr isotope data for the volcanic rocks are listed in Tables 2 and 3, respectively.

5.a. The age of basaltic andesites and rhyolite

Zircons separated from the basaltic andesite rocks (13TH03) are mostly colourless, transparent and well crystallized, with grain sizes of 100 to 200 μm diameter. CL images show that most of the zircons have a single composition and rhythmic zones typical of basic magmatic rocks, and some grains have dark and bright rims and black to dark cores, indicating that they are xenocrystic (Fig. 5a). SHRIMP U–Pb isotopic analytical results on zircon grains taken from the andesite sample are listed in Table 1 and are presented in Figure 5b. The samples are plotted along the concordant line with three groups of zircon U–Pb isotopic ages (Fig. 5b): 11 analysed zircons yield a $^{206}Pb/^{238}U$ weighted average age of 285.1 ± 5.9 Ma (MSWD = 2.3, $n = 11$), which we interpret as the crystallization age of the andesite; six analysed zircons yield a $^{206}Pb/^{238}U$ weighted average age of 357 ± 13 Ma (MSWD = 2.9, $n = 6$), and two zircon grains yield a $^{206}Pb/^{238}U$ age of 427 ± 7 Ma and 453 ± 10 Ma, respectively. These grains present quite complicated CL formations with dark or bright rims and black to dark cores, indicating that they are xenocrystic.

Zircons separated from the rhyolite (11TH04) are mostly colourless, transparent and well crystallized with grain sizes of 100 to 200 μm diameter, and CL images show that all of the zircons include special mottled patches with rhythmic zones (Fig. 5c). LA-ICP-MS U–Pb isotopic analytical data for zircon grains taken from the rhyolite sample are listed in Table 1 and are presented in Figure 5d. The samples concentrate in a small area along the concordia line (Fig. 5d), and 19 analysed zircons yield a $^{206}Pb/^{238}U$ weighted average age of 275.3 ± 1.8 Ma (MSWD = 1.8, $n = 19$).

An early Permian volcanism eruption was reported in the Turpan (Zhu *et al.* 2002) Basin and Shaerhu area of the Turpan Basin (285 Ma, Mao *et al.* 2014*c*; Table 4). Our analysis results show that the rhyolite erupted after the basaltic andesites, suggesting a *c.* 10 Ma volcanism eruption range of 285 to 275 Ma occurring in the early Permian.

5.b. Geochemical characteristics

Data on the major trace elements Rb–Sr and Sm–Nd are listed in Tables 2 and 3, respectively. Amygdale basalt, basaltic andesite and andesite show relatively variable high LOI (1.37–3.43 %), as the amygdales fill volatile-water-enriched minerals (e.g. carbonate and chlorite) not completely removed through the crushing process.

5.b.1 Major elements

The basalts present relatively high TiO_2 (2.14–2.59 %), CaO (8.01–8.85 %), MgO (5.37–6.53 %) and $Mg^{\#}$ (49.5–54.8) levels and lower alkali levels ($Na_2O + K_2O = 3.58–3.93$ %, $K_2O/Na_2O = 0.06–0.10$) and are classified as tholeiitic magma in a $FeO_t/MgO–SiO_2$ diagram (Fig. 6b; Myashiro, 1974). Compared to the basalt, the basaltic andesites (trachyandesite) present lower TiO_2 (1.13–1.45 %), CaO (2.18–3.43 %) and MgO (3.63–4.9 %, $Mg^{\#} = 48–58$) levels and higher alkali levels ($Na_2O + K_2O = 3.85–6.32$ %). The andesites (trachyandesites) present SiO_2 levels of 58.17 to 60.52 %, CaO levels of 8.01 to 8.85 %, MgO levels of 5.37 to 6.53 %, $Mg^{\#}$ levels

https://doi.org/10.1017/S0016756819001006 Published online by Cambridge University Press

Table 1. U–Pb SHRIMP and LA-ICP-MS isotopic data of zircon ages for the basaltic andesites and rhyolite from the Kalatage area in the Turpan Basin, NW China

13TH03: basalt–andesite by SHRIMP														
	Element contents (ppm) and ratio				Isotopic ratio						Isotopic age (Ma)			
Sample	U	Th	Pb (t)	Th/U	$^{207}Pb/^{206}Pb$	1σ (%)	$^{207}Pb/^{235}U$	1σ (%)	$^{206}Pb/^{238}U$	1σ (%)	$^{208}Pb/^{232}Th$	1σ	$^{206}Pb/^{238}U$	1σ
1	97	90	3.7	0.96	0.0508	17.3	0.3	17.5	0.0433	2.4	264	22	273.5	6.4
2	182	134	11.6	0.76	0.0542	6.6	0.54	7	0.0729	2.2	435	17	453.4	9.6
3	351	120	17.9	0.35	0.0497	7.7	0.4	7.9	0.0585	1.9	319	33	366.5	6.8
4	80	48	3.9	0.62	0.0446	20.7	0.34	20.9	0.0553	2.5	292	42	347.2	8.4
5	1743	1153	102.5	0.68	0.0552	1	0.52	2.1	0.0684	1.8	415	8	426.7	7.4
6	102	54	4	0.55	0.0558	14.7	0.34	14.8	0.0446	2.3	274	35	281.1	6.4
7	488	323	18.9	0.68	0.0532	6.9	0.33	7.2	0.0447	1.9	270	13	281.7	5.2
8	213	103	8.3	0.5	0.046	15.5	0.28	15.6	0.0441	2.1	269	33	278.4	5.7
9	350	193	17.2	0.57	0.0543	5.5	0.42	5.8	0.0567	1.9	368	17	355.5	6.6
10	588	675	24.4	1.19	0.0558	11.2	0.36	11.4	0.0469	2	335	15	295.4	5.7
11	157	205	6.3	1.35	0.0453	12.3	0.29	12.5	0.0457	2.2	279	12	288	6.1
12	167	119	8.5	0.73	0.0552	7.2	0.45	7.5	0.0591	2	357	18	369.9	7.3
13	365	187	14.2	0.53	0.0535	11.9	0.33	12.1	0.0447	2	291	29	281.7	5.6
14	252	92	10.1	0.38	0.0543	7.3	0.35	7.5	0.0463	2	273	21	291.5	5.7
15	275	164	10.3	0.62	0.047	7.5	0.28	7.7	0.0433	1.9	269	12	273	5.2
16	132	97	6.2	0.76	0.0465	14.8	0.34	15	0.0537	2.2	317	24	337.2	7.1
17	320	335	13.1	1.08	0.0482	7.8	0.31	8.1	0.0472	1.9	281	11	297.1	5.6
18	111	61	5.6	0.57	0.05	11.8	0.4	12	0.0578	2.2	335	32	362.2	7.7
19	163	180	6.6	1.14	0.051	7.2	0.33	7.5	0.0469	2	285	10	295.2	5.9
11TH04: rhyolite by LA-ICP-MS														
	Element contents (ppm) and ratio				Isotopic ratio						Isotopic age (Ma)			
Sample	U	Th	Pb (t)	Th/U	$^{207}Pb/^{206}Pb$	1σ	$^{207}Pb/^{235}U$	1σ	$^{206}Pb/^{238}U$	1σ	$^{207}Pb/^{235}U$	1σ	$^{206}Pb/^{238}U$	1σ
1	1473	848	114	0.58	0.06051	0.00216	0.35259	0.01158	0.04245	0.00039	306.7	8.7	268	2.4
2	348	234	38	0.67	0.05511	0.00192	0.33327	0.01108	0.04403	0.00041	292.1	8.4	277.7	2.5
3	345	146	23	0.42	0.054	0.00231	0.32563	0.01297	0.04406	0.00044	286.2	9.9	277.9	2.7
4	320	1160	19	3.63	0.05824	0.00256	0.35714	0.01718	0.0439	0.00052	310.1	12.9	277	3.2
5	1537	872	104	0.57	0.05632	0.00197	0.33461	0.01139	0.04296	0.00043	293.1	8.7	271.2	2.7
6	249	120	22	0.48	0.0512	0.00168	0.31322	0.00998	0.04433	0.0004	276.7	7.7	279.6	2.5
7	191	68	14	0.36	0.05397	0.00184	0.32836	0.01088	0.04429	0.00041	288.3	8.3	279.4	2.5
8	1420	938	109	0.66	0.05169	0.00171	0.30917	0.01024	0.0432	0.00041	273.5	7.9	272.6	2.6
9	1291	699	92	0.54	0.0552	0.00213	0.32847	0.01221	0.04351	0.00046	288.4	9.3	274.5	2.9
10	1202	728	94	0.61	0.05163	0.00178	0.31032	0.01062	0.04326	0.00043	274.4	8.2	273	2.7
11	1604	1148	126	0.72	0.05333	0.00172	0.32182	0.01006	0.04393	0.0004	283.3	7.7	277.1	2.5
12	1578	1050	121	0.67	0.051	0.00152	0.3095	0.00903	0.04381	0.00039	273.8	7	276.4	2.4
13	1527	980	113	0.64	0.04991	0.00166	0.306	0.00992	0.04421	0.00046	271.1	7.7	278.8	2.8
14	850	415	58	0.49	0.05351	0.00223	0.32037	0.01253	0.04361	0.00049	282.2	9.6	275.2	3
15	951	471	61	0.49	0.05183	0.00193	0.31147	0.01123	0.04393	0.00045	275.3	8.7	277.2	2.8
16	1309	784	93	0.6	0.05167	0.00251	0.3108	0.01703	0.04362	0.00044	274.8	13.2	275.2	2.7
17	914	458	71	0.5	0.05371	0.00206	0.31361	0.01188	0.04264	0.00049	277	9.2	269.2	3

https://doi.org/10.1017/S0016756819001006 Published online by Cambridge University Press

Table 2. Major (wt %) and trace element (ppm) data for the Permian volcanic rocks from the Kalatage area in the Turpan Basin, NW China

Sample	11TH05-1	11TH05-2	11TH05-7	11TH05-9	11TH03-13	11TH03-8	13KL50-2	13KL50-4	13KL50-5	11TH01-7	11TH01-9	11TH06-2	11TH06-3
Rock types	***Basalts***					***Basaltic andesites***					***Andesites***		
SiO_2	46.74	46.27	46.50	47.49	54.99	51.38	53.51	51.77	51.10	60.52	60.42	58.63	58.17
TiO_2	2.14	2.59	2.55	2.38	1.13	1.45	1.13	1.23	1.24	0.92	0.93	0.85	0.85
Al_2O_3	16.95	16.03	16.10	17.48	16.20	16.29	18.04	17.73	17.62	15.51	15.48	16.33	16.33
Fe_2O_{3T}	12.56	13.95	14.04	12.75	7.61	9.88	9.36	10.55	10.46	6.77	6.99	8.90	9.11
MnO	0.18	0.19	0.19	0.17	0.15	0.19	0.20	0.18	0.23	0.08	0.10	0.32	0.32
MgO	6.53	6.11	6.19	5.37	4.45	4.90	3.63	4.26	4.40	1.82	2.47	1.57	1.84
CaO	8.85	8.04	8.01	8.62	8.00	5.53	7.39	6.78	6.20	4.60	3.97	2.34	2.55
Na_2O	3.38	3.62	3.53	3.59	3.43	4.23	3.64	4.67	5.00	4.00	3.87	6.24	5.94
K_2O	0.20	0.31	0.34	0.34	0.42	2.09	0.51	0.24	0.24	3.97	3.82	2.52	2.55
P_2O_5	0.30	0.41	0.41	0.40	0.40	0.51	0.30	0.32	0.31	0.39	0.39	0.43	0.42
LOI	2.08	2.39	2.05	1.37	3.11	3.43	2.24	2.18	3.17	1.37	1.52	1.81	1.84
Total	99.91	99.91	99.91	99.96	99.89	99.88	99.95	99.92	99.98	99.95	99.96	99.94	99.92
$Mg^{\#}$	54.8	50.5	50.7	49.5	57.7	53.6	47.5	48.5	49.5	38.5	45.2	29.1	32.0
V	197	265	272	226	172	177	231	306	329	156	158	5.17	7.74
Cr	22.1	63.8	64.8	46.9	128	164	26.6	43.2	40.8	68.6	83.1	3.19	1.95
Co	52.5	51.3	51.8	43.3	26.3	34.8	27.6	35.8	34.5	19.1	23.1	2.52	2.68
Ni	72.5	59	62.9	50.8	52.5	80.5	21.8	25	24.8	35.9	39.4	0.691	0.653
Rb	1.65	1.87	2.03	1.95	3.33	41.4	5.32	1.75	1.85	51.8	54.2	27.1	27.9
Sr	523	363	365	403	647	581	497	489	504	922	1090	433	396
Y	36.4	42	41.6	37.8	27.4	38.2	29.3	29.2	29.8	24.3	25	68.7	73
Nb	3.07	4.43	4.31	4.07	4.67	8.87	3.71	3.77	3.8	4.37	4.33	10.8	11.3
Mo	0.28	0.79	0.48	0.44	0.28	1.08	0.90	0.39	0.55	0.73	0.82	1.45	1.67
Cs	0.88	1.66	1.41	0.34	0.85	0.69	0.14	0.23	0.16	0.36	0.47	0.51	0.57
Ba	110	105	101	97.2	388	1344	232	175	157	945	999	644	726
La	8.6	12.3	12.2	11.3	18.9	32.3	10.5	10.6	10.9	18.6	19.6	30.8	32.4
Ce	24.8	33.3	33	30.3	41.1	69.9	23.9	24.7	25.3	39.2	41.4	74.6	78.6
Pr	4.02	5.16	5.1	4.79	5.74	9.41	3.75	3.78	3.8	5.29	5.63	11.2	11.4
Nd	20	25.8	25.1	24	25.5	39.6	18.6	18.4	19.1	22.6	24.2	50.2	52.5
Sm	5.73	6.82	6.7	5.8	5.55	7.84	4.67	4.73	4.88	4.79	5.32	11.8	12
Eu	1.93	2.33	2.29	2.21	1.61	2.12	1.54	1.61	1.65	1.25	1.46	4.02	3.99
Gd	5.77	6.93	6.7	6.34	5.15	7.32	5.14	4.76	5.14	4.88	4.67	11.2	12
Tb	1.13	1.31	1.35	1.21	0.875	1.25	0.949	0.937	0.924	0.767	0.871	2.04	2.17
Dy	6.99	8.45	8.35	7.33	5.23	7.37	5.01	5.22	5.26	4.6	4.84	13.4	13.8
Ho	1.33	1.59	1.52	1.39	1.01	1.38	1.08	1.05	1.01	0.89	0.94	2.53	2.63
Er	4.19	4.83	4.43	4.13	3.05	3.88	3.09	3.13	3.3	2.62	2.72	7.87	8.19
Tm	0.60	0.70	0.71	0.63	0.48	0.64	0.51	0.45	0.48	0.39	0.50	1.24	1.31
Yb	3.75	4.64	4.64	4.07	2.97	3.82	3.48	2.83	3.32	2.63	2.65	8.41	8.81
Lu	0.60	0.70	0.70	0.62	0.46	0.62	0.46	0.42	0.46	0.38	0.44	1.32	1.37
Ta	0.19	0.37	0.31	0.25	0.26	0.50	0.16	0.18	0.21	0.24	0.25	0.58	0.57
Tl	0.08	0.06	0.03	0.02	0.01	0.19	0.02	0.04	0.02	0.20	0.21	0.05	0.06
Pb	1.41	1.98		1.56	4.13	8.19	2.19	2.43	2.48	5.80	5.24	6.42	7.20
Bi	0.01	0.02	0.01	0.01	0.02	0.03	0.01	0.01	0.01	0.04	0.10	0.01	0.01

(*Continued*)

https://doi.org/10.1017/S0016756819001006 Published online by Cambridge University Press

Table 2. (*Continued*)

Sample	11TH05-1	11TH05-2	11TH05-7	11TH05-9	11TH03-13	11TH03-8	13KL50-2	13KL50-4	13KL50-5	11TH01-7	11TH01-9	11TH06-2	11TH06-3
Rock types		***Basalts***				***Basaltic andesites***					***Andesites***		
Th	0.28	0.38	0.33	0.31	1.68	3.39	0.27	0.32	0.34	2.08	2.26	1.19	1.27
U	0.11	0.14	0.12	0.10	0.64	0.99	0.15	0.16	0.22	0.77	0.87	0.37	0.42
Zr	337	399	386	355	285	494	115	104	108	266	279	239	207
Hf	7.07	8.61	8.54	7.78	6.55	10.10	3.07	3.00	3.51	6.38	6.93	5.17	4.33
Nb/La	0.36	0.36	0.35	0.36	0.25	0.27	0.35	0.36	0.35	0.23	0.22	0.35	0.35
Sample	11TH06-6	13KL50-7	13KL50-10	11TH04-12	11TH04-13	13KL52-2	13KL52-3	11TH02-1	11TH02-3	11TH02-5	13TH01-1	13TH01-2	
Rock types		***Andesites***						***Rhyolites***					
SiO_2	58.24	58.47	59.62	73.07	73.73	72.61	73.94	83.54	80.98	82.27	82.36	82.48	
TiO_2	0.85	0.85	0.84	0.06	0.07	0.07	0.09	0.09	0.08	0.08	0.10	0.08	
Al_2O_3	16.37	18.20	17.21	12.64	12.14	13.00	13.35	8.86	8.15	7.97	8.83	8.59	
Fe_2O_{3T}	8.86	7.05	7.30	1.83	1.89	1.69	1.64	0.91	0.39	1.07	0.24	0.19	
MnO	0.34	0.16	0.12	0.06	0.05	0.05	0.07	0.02	0.02	0.07	0.02	0.01	
MgO	1.63	1.17	1.42	0.28	0.37	0.38	0.28	0.15	0.18	0.36	0.53	0.41	
CaO	2.23	4.19	4.99	0.76	0.86	0.36	0.67	0.51	2.66	1.64	1.05	1.19	
Na_2O	5.97	5.74	4.47	1.01	0.76	0.67	3.22	4.76	4.41	4.01	4.67	4.37	
K_2O	3.16	0.90	0.63	9.01	8.81	10.35	5.99	0.10	0.06	0.08	0.07	0.05	
P_2O5	0.43	0.46	0.43	0.01	0.01	0.01	0.01	0.01	0.01	0.01	0.02	0.02	
LOI	1.86	2.76	2.93	1.12	1.30	0.77	0.74	0.99	2.86	2.38	2.06	2.55	
Total	99.94	99.95	99.96	99.85	99.98	99.96	99.98	99.94	99.79	99.93	99.95	99.94	
$Mg^{\#}$	30.0	27.9	31.2	26.4	31.6	34.3	28.2	28.2	51.0	43.7	84.0	83.5	
V	6.55	83.1	75.9	9.53	11.3	3.11	5.02	19.1	22.5	22	9.33	7.49	
Cr	2.85	9.46	1.41	2.91	5.81	2.68	2.3	4.88	4.11	5.05	1.06	3.18	
Co	2.8	13.3	11.3	0.23	0.21	0.22	0.27	0.85	0.33	3.19	0.14	0.15	
Ni	1.01	7.91	2.71	0.735	0.623	2.19	0.898	1.33	1.4	3.99	0.32	1.70	
Rb	36.5	14.8	9.93	93.7	83.9	103	66.4	2.8	1.39	2.7	2.25	1.68	
Sr	491	430	450	86.5	90.6	49.3	115	63.8	107	126	96.10	146.00	
Y	77.3	39.6	33.7	66.7	67	83.8	75.3	34.7	33.2	21.6	39.20	36.90	
Nb	11.9	5.66	4.91	19.6	18.5	23.9	26.1	10.5	9.37	7.62	11.80	10.70	
Mo	1.41	1.82	0.76	0.35	0.54	0.50	0.58	0.52	0.11	0.13	10.80	9.05	
Cs	0.69	0.62	0.42	0.28	0.23	0.45	0.48	0.19	0.07	0.26	0.15	0.13	
Ba	782	370	280	1032	859	543	639	20.1	22.1	21.2	48.70	38.10	
La	34.2	16.4	15.4	40.9	36.6	38.2	41.2	19.5	12.7	4.54	18.40	15.30	
Ce	83.1	37.2	35.8	98	88.1	89.1	98.2	44.4	29.6	11.5	38.00	30.90	
Pr	12.2	5.57	5.37	13.8	12.4	12.8	13.8	5.92	4.47	1.67	5.57	4.38	
Nd	55.9	27.2	25.8	56.3	50.1	54.2	58.4	23.1	17.9	7.35	22.00	17.10	
Sm	12.7	6.37	6.13	12.9	11.1	12.9	14	4.81	3.97	2.23	5.46	4.30	
Eu	4.23	2	1.9	0.92	0.76	0.79	0.84	0.42	0.31	0.24	0.38	0.30	
Gd	12.4	6.66	6.1	12.1	9.82	13.4	13.3	4.33	3.81	2.16	4.99	4.46	
Tb	2.43	1.19	1.17	2.42	2.06	2.55	2.54	0.92	0.81	0.50	1.07	0.97	
Dy	14.4	7.04	6.43	14.9	12.6	14.9	14.8	5.94	4.98	3.1	6.55	5.95	
Ho	2.83	1.33	1.2	2.84	2.58	2.94	2.92	1.22	1.11	0.69	1.32	1.43	
Er	8.76	4.24	3.38	8.68	8.53	8.46	8.04	4.57	3.81	2.09	4.44	4.75	

(*Continued*)

https://doi.org/10.1017/S0016756819001006 Published online by Cambridge University Press

Table 2. (*Continued*)

Sample	11TH06-6	13KL50-7	13KL50-10	11TH04-12	11TH04-13	13KL52-2	13KL52-3	11TH02-1	11TH02-3	11TH02-5	13TH01-1	13TH01-2
Rock types		***Andesites***						***Rhyolites***				
Tm	1.34	0.71	0.58	1.49	1.59	1.44	1.19	0.75	0.64	0.32	0.72	0.69
Yb	8.94	4.01	3.62	10.30	10.50	9.32	8.05	4.98	3.95	2.18	4.45	3.90
Lu	1.40	0.58	0.51	1.67	1.64	1.33	1.23	0.70	0.58	0.33	0.65	0.64
Ta	0.57	0.29	0.31	1.12	1.04	1.53	1.55	0.62	0.57	0.48	1.11	0.95
Tl	0.05	0.07	0.04	0.86	0.89	0.90	0.78	0.03	0.03	0.02	0.09	0.06
Pb	7.34	3.49	3.66	13.60	9.74	17.30	17.50	4.77	3.83	3.03	4.80	4.46
Bi	0.02	0.02	0.05	0.03	0.04	0.14	0.15	0.03	0.03	0.05	0.02	0.01
Th	1.28	0.57	0.55	4.44	4.08	4.03	4.26	11.30	10.10	7.94	9.34	6.49
U	0.42	0.28	0.30	1.72	1.54	1.49	1.57	3.55	2.65	2.32	2.20	2.27
Zr	245	180	161	739	685	446	454	252	207	191	152.00	139.00
Hf	4.76	4.73	4.46	26.00	23.80	16.20	16.70	8.53	7.45	6.29	6.89	5.36
Nb/La	0.35	0.35	0.32	0.48	0.51	0.63	0.63	0.54	0.74	1.68	0.64	0.70

of 49.5 to 54.8, alkali levels of $Na_2O + K_2O = 5.10–9.13$ %, $K_2O/Na_2O = 0.14–0.99$ and low TiO_2 levels of 0.84 to 0.93 %. They are metaluminous with A/CNK values of between 0.81 and 1.01.

The rhyolites are highly siliceous ($SiO_2 = 72.61–83.54$ %), rich in total alkalis ($Na_2O + K_2O = 4.09–11.02$ %), but low in Al and Ti, with $Al_2O_3 = 7.97–13.35$ % and $TiO_2 = 0.06–0.10$ %. The rhyolites have relatively low ferromagnesian compositions ($MgO = 0.15–0.53$ % and $Fe_2O_3t = 0.19–1.89$ %). They are metaluminous to weakly peraluminous with A/CNK values ranging from 0.67 to 1.03 and with A/NK values ranging from 1.06 to 1.19 (Table 2). The rhyolites can be divided into low- and high-silica types with apparent geochemical differences between them and with SiO_2 levels ranging from 72.61 to 73.94 % (11TH04 and 13KL52) and from 80.98 to 83.54 % (11TH02 and 13TH01), respectively. The high-silica samples present obviously lower K_2O and Al_2O_3 levels than the low-silica samples ($K_2O = 0.05–0.10$ % and 5.99–10.35 % and $Al_2O_3 = 7.97–8.86$ % and 5.99–10.35 % respectively), showing that the high-silica rocks underwent an advanced fractionation of K-feldspar. In summary, the different types of volcanic rock are alkaline to subalkaline series magma, and the SiO_2 content of the samples ranges from 46.27 % to 83.54 % (Fig. 5). The samples are classified as basalts, basaltic andesites (basaltic trachyandesites), andesites (trachyandesites) and rhyolites in a total alkali–silica (TAS) diagram (Fig. 6a; Le Maitre *et al.* 1989), and the basalts and basaltic andesites are composed of tholeiitic series magma (Fig. 6b; Myashiro, 1974). As demonstrated by the binary diagrams (Figs 6, 7), the rocks show positive correlations between SiO_2 and TiO_2, Al_2O_3, CaO, MgO, MnO, P_2O_5, Cr, Ni, Co and Sr levels and negative correlations between SiO_2 and K_2O, Y and Zr levels.

5.b.2. Trace and rare-earth elements

The basalts display uniform enrichment of light rare earth elements (LREEs) across the chondrite-normalized REE plots with $(La/Yb)_N$ ratios of 1.65 to 1.99 (Fig. 8a). They show slightly positive Eu anomalies ($\delta Eu = 1.03–1.11$), suggesting that plagioclase fractionated and accumulated throughout the evolution of the parental magma. In the primitive mantle-normalized spider diagram (Fig. 8b), basalts are characterized by low HFSE (high-field-strength elements)/LREE ratios ($Nb/La = 0.35–0.36$); an enrichment of Pb, Sr, Zr and Hf; and relatively negative Rb, Th, U, Nb and Ta anomalies. These features are similar to those of continental N-MORB/E-MORB-type basalts (Condie, 1989; Wilson, 1989), suggesting that the extension of basins reached maximum levels in middle and late stages of extensional volcanic movement.

The basaltic andesites display LREE enrichment chondrite-normalized REE patterns ($(La/Yb)_N = 2.16–6.07$) with slightly negative to positive Eu anomalies ($\delta Eu = 0.86–1.04$) (Fig. 8c). In the primitive mantle-normalized spider diagram, the samples show a moderate enrichment of large-ion lithophile elements (LILE; e.g. Rb, Ba, U, Th, K and Sr), Pb, Zr and Hf elements and negative Nb, Ta and Ti anomalies (Fig. 8d).

The andesites present REE and trace element chemical features similar to those of the basaltic andesites with LREE enrichment chondrite-normalized REE patterns ($(La/Yb)_N = 2.63–5.31$) and slightly negative to positive Eu anomalies ($\delta Eu = 0.79–1.07$) (Fig. 8e). The samples are characterized by an enrichment of LREE, Rb, Ba, Th, U, K, Pb elements and by relatively negative Nb, Ta and Ti anomalies in the primitive mantle-normalized spider diagram (Fig. 8f).

Rhyolites are highly fractionated magmas with high silica, high alkali, low TiO_2 and ferromagnesian compositions. The chondrite-normalized REE plot yields two tightly clustered groups where low-silica rhyolites present higher REE levels and more enriched Rb, Ba, K, Pb, Zr and Hf elements (Fig. 8g, h). The high-silica rhyolites display depleted Rb, Ba and K levels, suggesting that the rocks underwent varying degrees of K-feldspar fractionation. They are characterized by tetrad effect patterns (V and/or M type) (Zhao *et al.* 1992, 2002; Jahn *et al.* 2001) (Fig. 8g) with a strong negative Eu anomaly ($Eu/Eu^* = 0.18–0.33$). The samples are characterized by non-CHARAC (charge-and-radius-controlled) trace element behaviours with Rb, K, Pb, Zr and Hf enrichment; relatively high negative Nb anomalies; pronounced negative Ba, Sr and Eu anomalies consistent with feldspar fractionation; and negative Ti anomalies with titanite/ilmenite fractionation (Fig. 8h). These trace features may be attributed to intense interactions between high-fractionation magmas and aqueous hydrothermal fluids (likely rich in F and Cl) (Zhao *et al.* 1992, 2002; Jahn *et al.* 2001).

https://doi.org/10.1017/S0016756819001006 Published online by Cambridge University Press

Table 3. Sm–Nd and Rb–Sr isotopic analytical results of the Permian volcanic rocks from Kalatage area in the Turpan Basin, NW China

Samples	Rb (10^{-6})	Sr (10^{-6})	$^{87}Rb/^{86}Sr$	$^{87}Sr/^{86}Sr$	2σ	$(^{87}Sr/^{86}Sr)_i$	Sm ($\times10^{-6}$)	Nd (10^{-6})	$^{147}Sm/^{144}Nd$	$^{143}Nd/^{144}Nd$	(2σ)	$(^{143}Nd/^{144}Nd)_i$	εNd (t)	T_{DM}	T_{2DM}	T (Ma)
Basalts																
11TH05-2	2.39	653.9	0.0106	0.703677	0.000008	0.70363	5.965	25.84	0.1398	0.512895	0.000011	0.512634	7.1	529	474	285
11TH05-1	1.815	373.4	0.0141	0.703475	0.000015	0.70342	6.551	24.56	0.1615	0.512964	0.000009	0.512663	7.6	548	428	285
Basaltic andesites																
11TH03-8	40.05	608.4	0.1905	0.705056	0.000015	0.70428	7.505	35.3	0.1287	0.512745	0.000011	0.512505	4.6	729	680	285
Andesites																
11TH06-2	29.65	493.7	0.1738	0.704715	0.00001	0.70401	11.9	50.32	0.1431	0.512956	0.000013	0.512689	8.2	422	386	285
11TH01-7	55.19	1152	0.1387	0.70446	0.000013	0.70390	5.002	22.91	0.1322	0.51287	0.000013	0.512623	6.9	527	491	285
Rhyolites																
11TH04-13	85.14	94.29	2.616	0.716519	0.000013	0.70591	11.33	48.44	0.1416	0.512921	0.000011	0.512657	7.5	488	438	285
11TH02-1	25.56	383	0.1929	0.705334	0.000012	0.70522	3.74	19.3	0.1174	0.512792	0.000006	0.512533	5.1	696	635	285
Shaerhu complex (Mao *et al.* 2014)																
Gabbro-09SF02	49.8	257	0.5611	0.706399	0.000013	0.70416	12.52	61.9	0.1223	0.512861	0.000006	0.512637	7.0	485	476	285
Granite-09SF10	87	29.1	8.6582	0.735978	0.000013	0.70148	8.01	29.1	0.1666	0.513158	0.000007	0.512853	11.2		131	285
Rhyolite-09SF17	5.08	353	0.0417	0.703462	0.000011	0.70330	5.21	19.52	0.1614	0.512983	0.000005	0.512687	8.0	491	395	285

In summary, these volcanic rocks are characterized by variable LREE-enriched patterns ($(La/Yb)_N = 1.49–6.07$), a range of slightly positive to highly negative Eu anomalies ($Eu/Eu^* = 0.18–1.11$) and relatively more depleted Nb, Ta, P and Ti elements from basalt to rhyolite (Fig. 8). These features suggest that plagioclase played an important role in partial melting and subsequent fractional crystallization.

5.b.3. Sr–Nd isotope

The Permian volcanic rocks have $^{87}Rb/^{86}Sr$ ratios of 0.0106 to 2.616, $^{87}Sr/^{86}Sr$ ratios of 0.70348 to 0.71652 and a relatively low initial Sr ($(^{87}Sr/^{86}Sr)_i = 0.70342–0.70591$, $i = 285$ Ma). They have $^{147}Sm/^{144}Nd$ ratios of 0.1174 to 0.1615, high $^{143}Nd/^{144}Nd$ ratios of 0.51275 to 0.51296 and relatively high $(^{143}Nd/^{144}Nd)_i$ (0.51250–0.51269) and $\epsilon_{Nd}(t)$ (4.6–8.2, $t = 285$ Ma) values (Fig. 9). The basalts are characterized by the highest $\epsilon_{Nd}(t)$ ($\epsilon_{Nd}(t) = 7.1–7.6$) values and the lowest $(^{87}Sr/^{86}Sr)_i$ ratios ($(^{87}Sr/^{86}Sr)_i = 0.70342–0.70363$) (Fig. 9). Basaltic andesites present the lowest $\epsilon_{Nd}(t)$ value of 4.6 and moderate $(^{87}Sr/^{86}Sr)_i$ ratios ($(^{87}Sr/^{86}Sr)_i = 0.70428$) (Fig. 9). Andesites present moderate $\epsilon_{Nd}(t)$ values of 6.9 to 8.2 and $(^{87}Sr/^{86}Sr)_i$ ratios of ($(^{87}Sr/^{86}Sr)_i = 0.70390–0.70401$) (Fig. 9). Rhyolites present moderate $\epsilon_{Nd}(t)$ values ranging from 5.1 to 7.5 and the highest $(^{87}Sr/^{86}Sr)_i$ ratios ($(^{87}Sr/^{86}Sr)_i = 0.70522–0.70591$) (Fig. 9). In summary, the volcanic rocks display high $\epsilon_{Nd}(t)$ values that vary little and strong variations in $(^{87}Sr/^{86}Sr)_i$ ratios.

6. Discussion

6.a. Petrogenesis of Permian volcanic rocks

The mafic rocks are tholeiitic in nature. Their relatively high $Mg^{\#}$ values (48–58) together with their MgO (5.37–6.53 wt %), Cr (22–65 ppm) and Ni content (51–73 ppm) indicate that mafic magmas of the Turpan Basin were derived from a mantle source and may have been produced from variably fractionated melts and not from primitive magmas. In addition, the basalts are enriched with LREEs, LILEs (e.g. Ba, K and Sr), Pb, Zr, Hf and elements depleted of HFSE (e.g. Nb ($Nb/La = 0.35–0.36$) and Ta), strongly suggesting a subduction zone origin/arc affinity and resembling primitive arc tholeiites (Pearce & Cann, 1973). According to the Th/Yb vs Nb/Yb diagram (Fig. 10a; Pearce, 1982, 2008), the samples fall obliquely, crossing the mantle array and showing that the samples evolved from N-MORB (normal mid-ocean ridge basalt)-like sources with a significant degree of fractional crystallization (FC) coupled with assimilation by low radiogenic Sr but high Th levels. Moreover, the basalts display relatively high $\epsilon_{Nd}(t)$ ($\epsilon_{Nd}(t) = 7.1–7.6$) values; low $(^{87}Sr/^{86}Sr)_i$ ratios ($(^{87}Sr/^{86}Sr)_i = 0.70342–0.70363$); and depleted Rb, Th and U elements (Fig. 8b), suggesting derivation from a depleted mantle source. The Tb (or Sm)/Yb ratio can be used to estimate the depth of melting, as it is insensitive to the effects of fractional crystallization (McKenzie & O'Nions, 1991; K Wang *et al.* 2002). The basalt to andesite samples have low $(Tb/Yb)_P$ (1.12–1.51 < 1.80) ratios, clearly showing that melting occurred in the absence of garnet (K Wang *et al.* 2002). In the $(La/Yb)_p$ vs $(Tb/Yb)_P$ diagram (Fig. 10b), our data fall below the garnet–spinel transition line for peridotite and present nearly flat to slightly fractionated chondrite-normalized heavy rare earth elements (HREE) patterns ($(La/Yb)_N = 1.65–6.07$), indicating that primitive magma from these rocks may have originated from a garnet-free mantle. In conclusion, it is inferred that the

https://doi.org/10.1017/S0016756819001006 Published online by Cambridge University Press

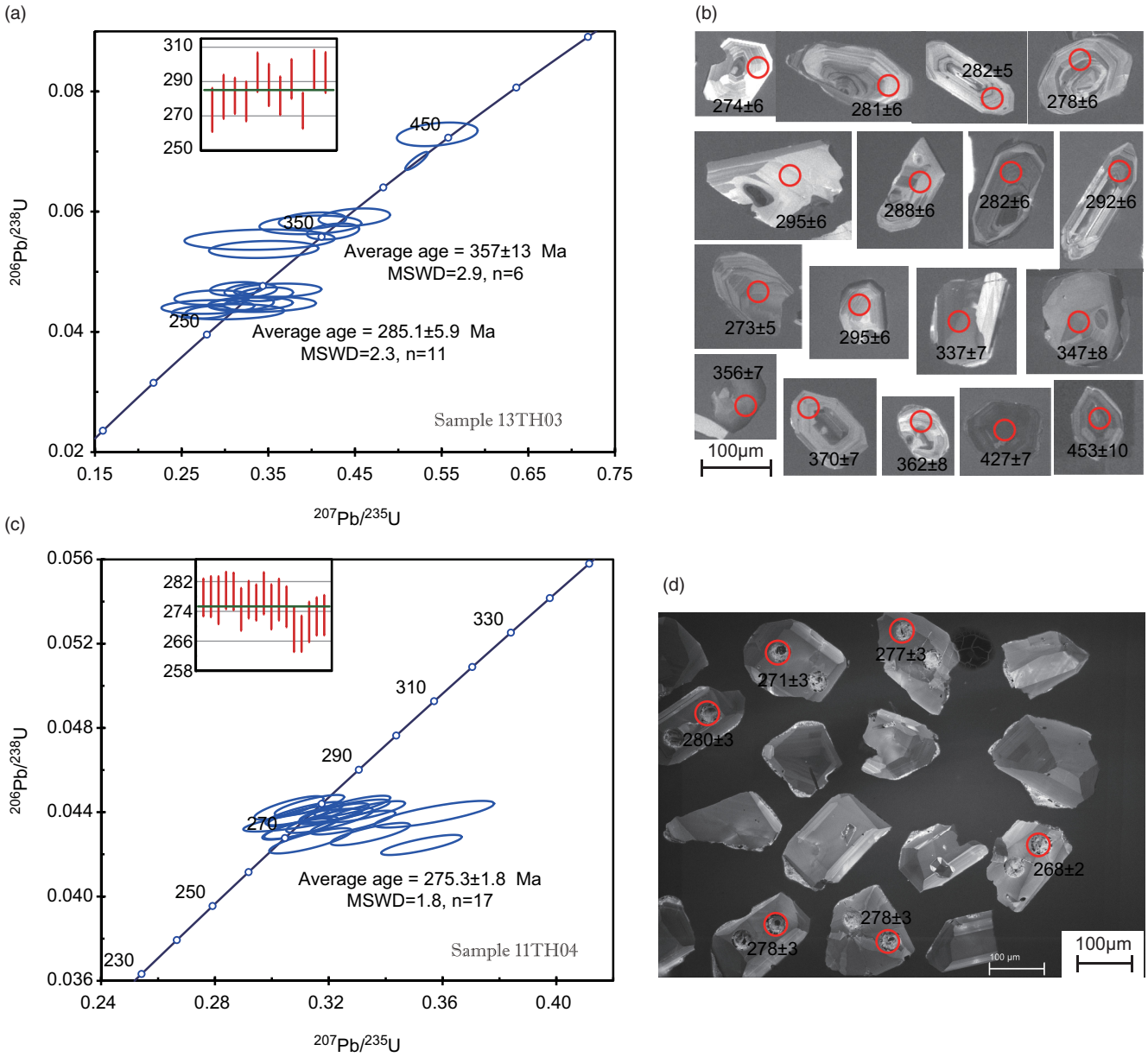

Fig. 5. CL images of typical zircons and concordia U–Pb diagram for rhyolites and basaltic andesites from the Kalatage area in the Turpan Basin. (a, b) CL images and LA-ICP-MS analytical data for the basaltic andesite (13TH03); (c, d) CL images and SHRIMP analytical data for the rhyolite (11TH04).

petrogenesis of the mafic rocks was dominated by a process of mixing between basaltic magmas similar to MORBs from asthenospheric (depleted end-member mantle) and arc-like magmas (Wilson, 2001; Condie, 2005). Basaltic andesites and andesites have arc-related geochemical characteristics that display moderate TiO_2 levels; LREE enrichment; LILE (e.g. Rb, Ba, U, Th, K and Sr), Pb, Zr and Hf elements; negative Nb, Ta and Ti anomalies; negative Nb, Ta and Ti anomalies; slightly negative to positive Eu anomalies (δEu = 0.86–1.04); high $\epsilon_{Nd}(t)$ values of 4.6 to 8.2; and moderate $(^{87}Sr/^{86}Sr)_i$ ratios ($(^{87}Sr/^{86}Sr)_i$ = 0.70390–0.70428). Most of the basalt, basaltic andesite and andesite samples plot from the arc to N-MORB basalt fields in the Hf–Th–Nb discrimination diagrams (Fig. 11a) and in the volcanic arc basalt (VAB) and MORB fields in the Ce/Sr–Cr discrimination diagrams, suggesting that these rocks formed in a supra-subduction zone setting. All of these features indicate that the basalts, basaltic andesites and andesite rocks are mantle-derived and formed at the extensional basin in a supra-subduction zone setting.

The rhyolites are highly siliceous and high in total alkali levels. In general, the rocks are variably enriched with HFSE and REE. The geochemical characteristics of rhyolites, including high SiO_2, $K_2O + Na_2O$, Fe/Mg, Ga, Zr, Nb, Y and REE levels, show an affinity with A-type granites (Loiselle & Wones, 1979; Whalen *et al.* 1987). According to the geochemical subdivision of A-type granites illustrated by Eby (1992), including relatively high Y/Nb ratios (2.84–3.62), the rhyolites belong to the A_2 subtype (Fig. 10c). In the discrimination diagrams (Fig. 11d), the rhyolite samples plot from the volcanic arc to the plate granite field, suggesting that the rhyolites formed in a supra-subduction zone setting.

The direct fractionation of mantle-derived tholeiitic magmas constitutes an important source of A-type felsic rock petrogenesis

https://doi.org/10.1017/S0016756819001006 Published online by Cambridge University Press

Table 4. The ages of early Permian volcanic rocks and mafic–ultramafic intrusions from Altai to Beishan in China

Location	Rock type	Analysed mineral	Analysis method	Age(Ma)	Reference
1. Huangshan–Jingerquan-					
Huangshandong	Norite	Zircon	SHRIMP	274 ± 3	Han *et al.* (2004)
Huangshan	Gabbro	Zircon	SIMS	283.8 ± 3.4	Qin *et al.* (2011)
	Diorite	Zircon	SHRIMP	269 ± 2.1	Zhou *et al.* (2004)
Xiangshan	Gabbro	Zircon	SIMS	279.6 ± 1.1	Han *et al.* (2004)
Hulu	Diorite	Zircon	LA-ICP-MS	274.5 ± 3.9	Sun *et al.* (2010)
2. Baishiquan		Zircon			
Baishiquan	Gabbro	Zircon	LA-ICP-MS	280.4 ± 1.4	Mao *et al.* (2006)
	Diorite	Zircon	SHRIMP	285 ± 10	Wu *et al.* (2005)
	Gabbro	Zircon	SHRIMP	284.4 ± 8	Wu *et al.* (2005)
	Gabbro–diorite	Zircon	SHRIMP	284 ± 9	Wu *et al.* (2005)
3. Haibaotan area					
Haibaotan	Gabbro	Zircon	SHRIMP	269.2 ± 3.2	JY Li *et al.* (2006*b*)
Baixingtan	Plagioclase-bearing wehrlite	Zircon	LA-ICP-MS	277.9 ± 2.6	Wang *et al.* (2015)
4. Lubei-Qiatekaer		Zircon			
Qiatekaer	Gabbro	Zircon	SHRIMP	277 ± 1.6	JY Li *et al.* (2006*b*)
5. Pobei-Cihai		Zircon			
Pobei No. 1 intrusion	Olivine gabbro	Zircon	SIMS	284 ± 2.2	Qin *et al.* (2011)
	Gabbro	Zircon	SHRIMP	278 ± 2	WQ Li *et al.* (2006)
	Gabbro	Zircon	LA-ICP-MS	283.8 ± 1.1	Ao *et al.* (2010)
Hongshishan	Olivine gabbro	Zircon	LA-ICP-MS	281.8 ± 2.6	Ao *et al.* (2010)
Bijiashan	Gabbro	Zircon	SIMS	279.2 ± 2.3	Qin *et al.* (2011)
Chihai area	Gabbro	Zircon	LA-ICP-MS	276.1 ± 0.63	Meng *et al.* (2014)
	Basalt	Zircon	SHRIMP	277 ± 6	Li *et al.* (2012)
6. Kalatongke		Zircon			
Kalatongke	Norite	Zircon	SHRIMP	287 ± 5	Han *et al.* (2004)
1. Turpan basin		Zircon			
Shaerhu area	Rhyolite	Zircon	SIMS	286.7 ± 2.1	Mao *et al.* (2014)
Shaerhu area	Gabbro	Zircon	SIMS	286.5 ± 2.1	
South to Kalatage area	Andesite	Zircon	LA-ICP-MS	285.1 ± 5.9	This study
South to Kalatage area	Rhyolite	Zircon	LA-ICP-MS	275.3 ± 1.8	This study
Dananhu area	Basalt	Whole rock	Ar–Ar	270 ± 1	Zhou *et al.* (2006)
Turpan Basin	Basalt	Whole rock	Ar–Ar	278 ± 1	Zhou *et al.* (2006)
Turpan Basin	Basalt	Whole rock	Ar–Ar	281 ± 1	Zhou *et al.* (2006)
Turpan Basin	Basalt	Whole rock	Ar–Ar	293 ± 2	Zhou *et al.* (2006)
Hami Basin	Basalt	Whole rock	Ar–Ar	290 ± 1	Zhou *et al.* (2006)
2. Bogda-Haerlik Mountain					
Baiyanggou	Basalt	Zircon	LA-ICP-MS	295.8 ± 2.8	Chen *et al.* (2011)
	Rhyolite	Zircon	LA-ICP-MS	293.3 ± 1.7	Chen *et al.* (2011)
Qijiaojing	Rhyolite	Zircon	LA-ICP-MS	294.6 ± 2	Chen *et al.* (2011)
Hongshankou	Rhyolite	Zircon	LA-ICP-MS	293.6 ± 2.2	Chen *et al.* (2011)
Cheguluquan	Rhyolite	Zircon	LA-ICP-MS	293.6 ± 2.3	Chen *et al.* (2011)
	Basalt	Zircon	LA-ICP-MS	294.5 ± 3.6	Chen *et al.* (2011)

(*Continued*)

https://doi.org/10.1017/S0016756819001006 Published online by Cambridge University Press

Table 4. (*Continued*)

Location	Rock type	Analysed mineral	Analysis method	Age(Ma)	Reference
South margin of Bogda Mountain	Basalt	Whole rock	Ar–Ar	273 ± 1	Zhou *et al.* (2006)
	Basalt	Whole rock	Ar–Ar	276 ± 2	Zhou *et al.* (2006)
	Basalt	Whole rock	Ar–Ar	270 ± 1	Zhou *et al.* (2006)
South margin of Haerlik Mountain	Basalt	Whole rock	Ar–Ar	269 ± 1	Zhou *et al.* (2006)
	Basalt	Whole rock	Ar–Ar	276 ± 1	Zhou *et al.* (2006)
	Basalt	Whole rock	Ar–Ar	291 ± 1	Zhou *et al.* (2006)
3. Santanghu Basin					
	Basalt	Whole rock	Ar–Ar	266 ± 1	Zhou *et al.* (2006)
	Basalt	Whole rock	Ar–Ar	272 ± 1	Zhou *et al.* (2006)
	Basalt	Whole rock	Ar–Ar	273 ± 1	Zhou *et al.* (2006)
	Basalt	Whole rock	Ar–Ar	266 ± 1	Zhou *et al.* (2006)
	Tuff	Zircon	SIMS	286.1 ± 3.6	Wang (2013)
	Andesite	Zircon	LA-ICP-MS	269.4 ± 5.9	Wang (2013)
4. Hongliuhe area					
	Basalt	Whole rock	Ar–Ar	278 ± 17	Pan *et al.* (2008)
5. Liuyuan area					
	Gabbro dike	Zircon	LA-ICP-MS	286 ± 2	Mao *et al.* (2012)
	Diorite dike	Zircon	SHRIMP	272.7 ± 4.4	Zhang *et al.* (2011)
	Diorite dike	Zircon	SHRIMP	291.4 ± 4.9	Zhang *et al.* (2011)
6. Wulunguhe					
Zaheba area	Rhyolite	Zircon	SHRIMP	279.8 ± 2.5	Li *et al.* (2013)
Zaheba area	Rhyolite	Zircon	SHRIMP	276 ± 3	Li *et al.* (2013)
Zaheba area	Rhyolite	Zircon	SHRIMP	276.2 ± 3.1	Li *et al.* (2013)
Qiakuertu	Rhyolite	Zircon	LA-ICP-MS	279.5 ± 1.4	Tang *et al.* (2018)
Qiakuertu	Basalt	Zircon	LA-ICP-MS	280.4 ± 1.3	Tang *et al.* (2018)

SIMS: secondary ice mass spectrometry.

(Bonin *et al.* 1978; Turner *et al.* 1992; Han *et al.* 1997; Hollings *et al.* 2004; Mao *et al.* 2014*c*). The series of volcanic rocks in the Turpan Basin exhibit high $\epsilon_{Nd}(t)$ values, and rhyolites present $\epsilon_{Nd}(t)$ values of 5.1 to 7.5, suggesting that the rhyolites derived from the mantle. The relatively strong negative Eu anomaly (Eu/Eu* = 0.18–0.33) and spectacular tetrad effects observed from their REE distribution patterns suggest that extensive magmatic differentiation played an important role in magmatic processes, during which intense interactions between the highly evolved magmas and aqueous hydrothermal fluids (likely rich in F and Cl) formed typical trace elements and REE distributions (Zhao *et al.* 1992, 2002; Jahn *et al.* 2001). Fractionation trends observed in the magmatic suite are also clearly indicated by the rhyolitic rocks with their striking depletions of Ba, Sr, P, Ti and Eu as shown from the spidergrams and REE patterns (Fig. 8). The rhyolites present low MgO, Cr, Ni and Co levels, consistent with the highly differentiated nature of the magmas, which can be attributed to pyroxene and amphibole fractions. Strong differences in K_2O, Al_2O_3, Zr, Nb and Y content levels of the two groups of rhyolites also suggest that the rocks underwent varying degrees of K-feldspar and zircon fractionation.

Our studies reveal that the studied series of volcanic rocks present SiO_2 content levels of 46.27 % to 83.54 % (Fig. 6), containing basalts, basaltic andesites (trachyandesites), andesites (trachyandesites) and rhyolites. Significant degrees of fractionation are recorded from the geochemistry of the volcanic rocks, including those illustrated by the binary diagrams (Fig. 7). The rocks show positive correlations between SiO_2 and K_2O and Rb levels and negative correlations between SiO_2 and CaO, Al_2O_3, MgO, TiO_2, P_2O_5, Co, Ni, V, Co and Sr levels, indicating that the volcanic rocks originate from the same source and that magmatic differentiation was central to their generation as exemplified by the fractionation of clinopyroxene, amphibole, ilmenite, apatite and plagioclase. Fractionation trends observed in the magmatic suite are also clearly indicated by variable LREE levels; slightly positive to highly negative Eu anomalies (Eu/Eu* = 0.86–1.00); and more depleted Nb, Ta, P and Ti elements originating from basalts to rhyolites observed from the samples. For example, negative Eu depletion requires magmas to undergo extensive feldspar fractionation, and a negative Ti anomaly is often related to ilmenite fractionation while a negative P anomaly is attributed to apatite

https://doi.org/10.1017/S0016756819001006 Published online by Cambridge University Press

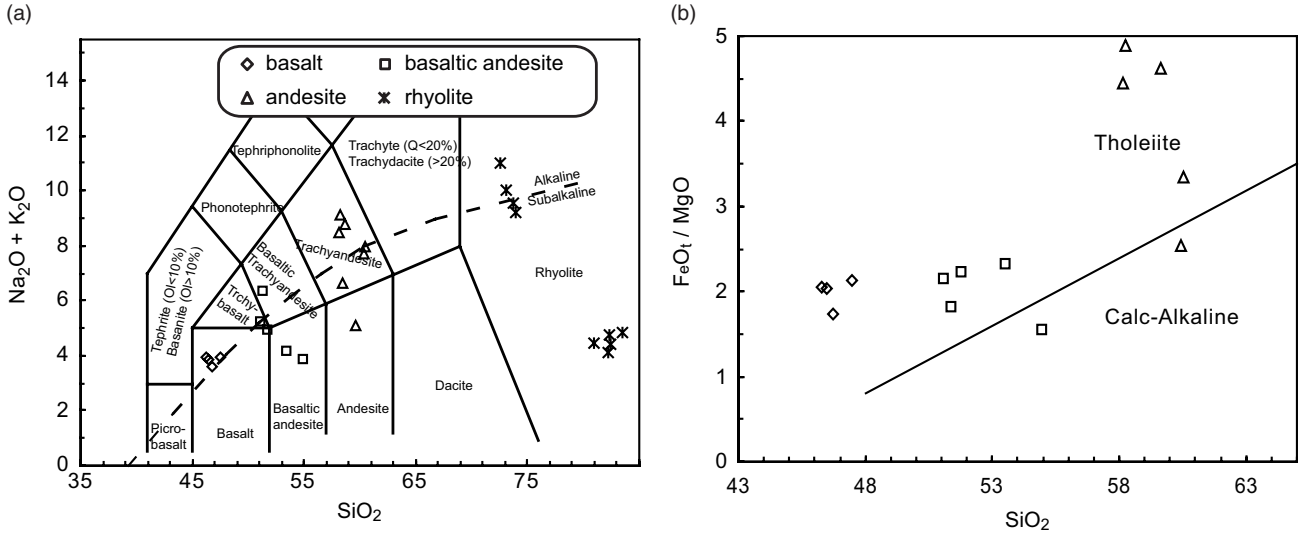

Fig. 6. Geochemical classification diagrams for the Permian volcanic rocks from the Kalatage area in the Turpan Basin. (a) SiO_2 (wt %) vs $K_2O + Na_2O$ (TAS, wt %) diagram (Le Maitre *et al.* 1989). The boundary line between alkaline and tholeiitic rocks based on Irvine & Baragar (1971). (b) FeO_t/MgO vs SiO_2 diagram (Myashiro, 1974).

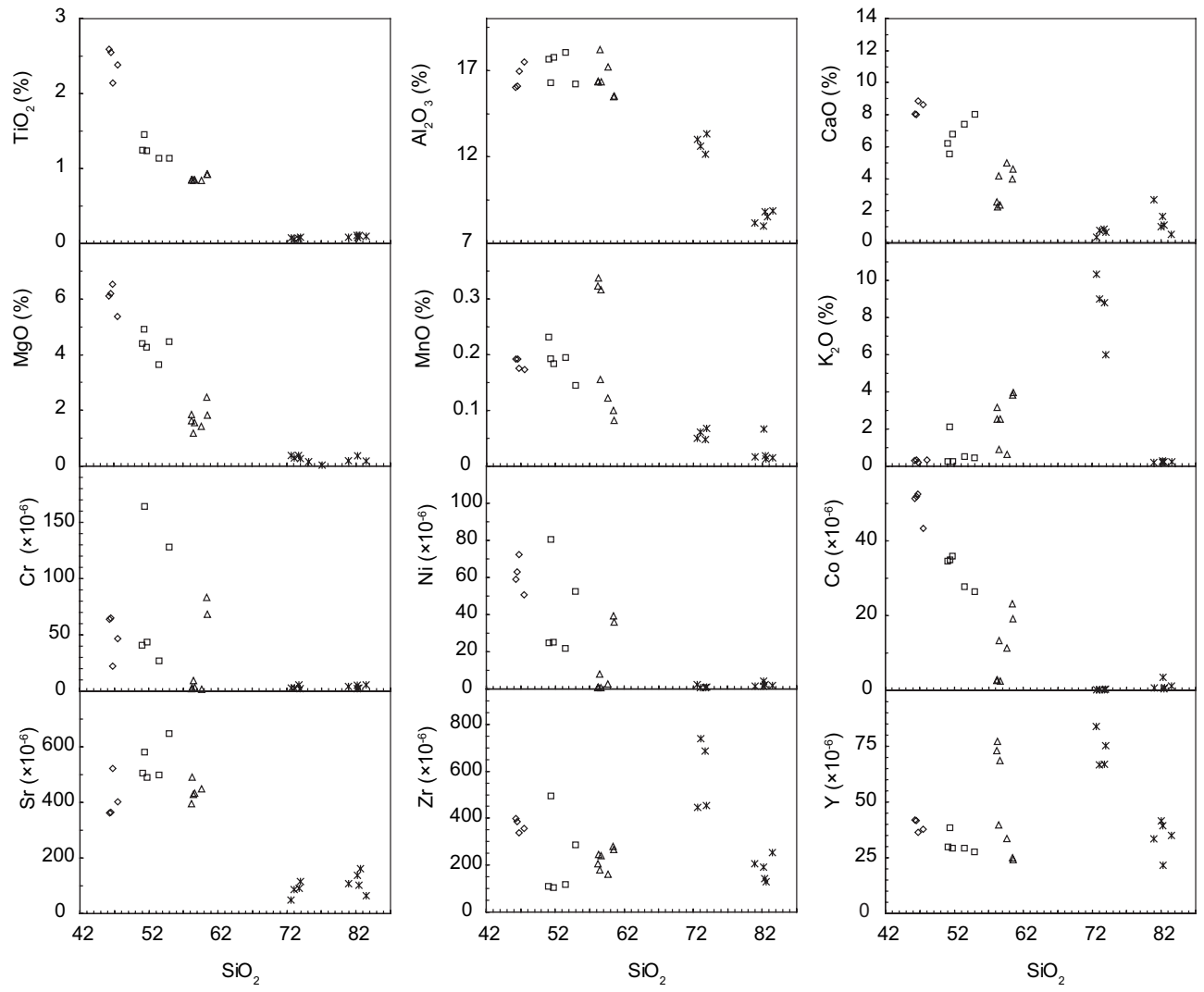

Fig. 7. Binary diagrams illustrating SiO_2 vs major and trace elements of Permian volcanic rocks from the Kalatage area in the Turpan Basin. Values are given in wt % for oxides and in ppm for trace elements. Symbols used are the same as those used in Figure 6.

https://doi.org/10.1017/S0016756819001006 Published online by Cambridge University Press

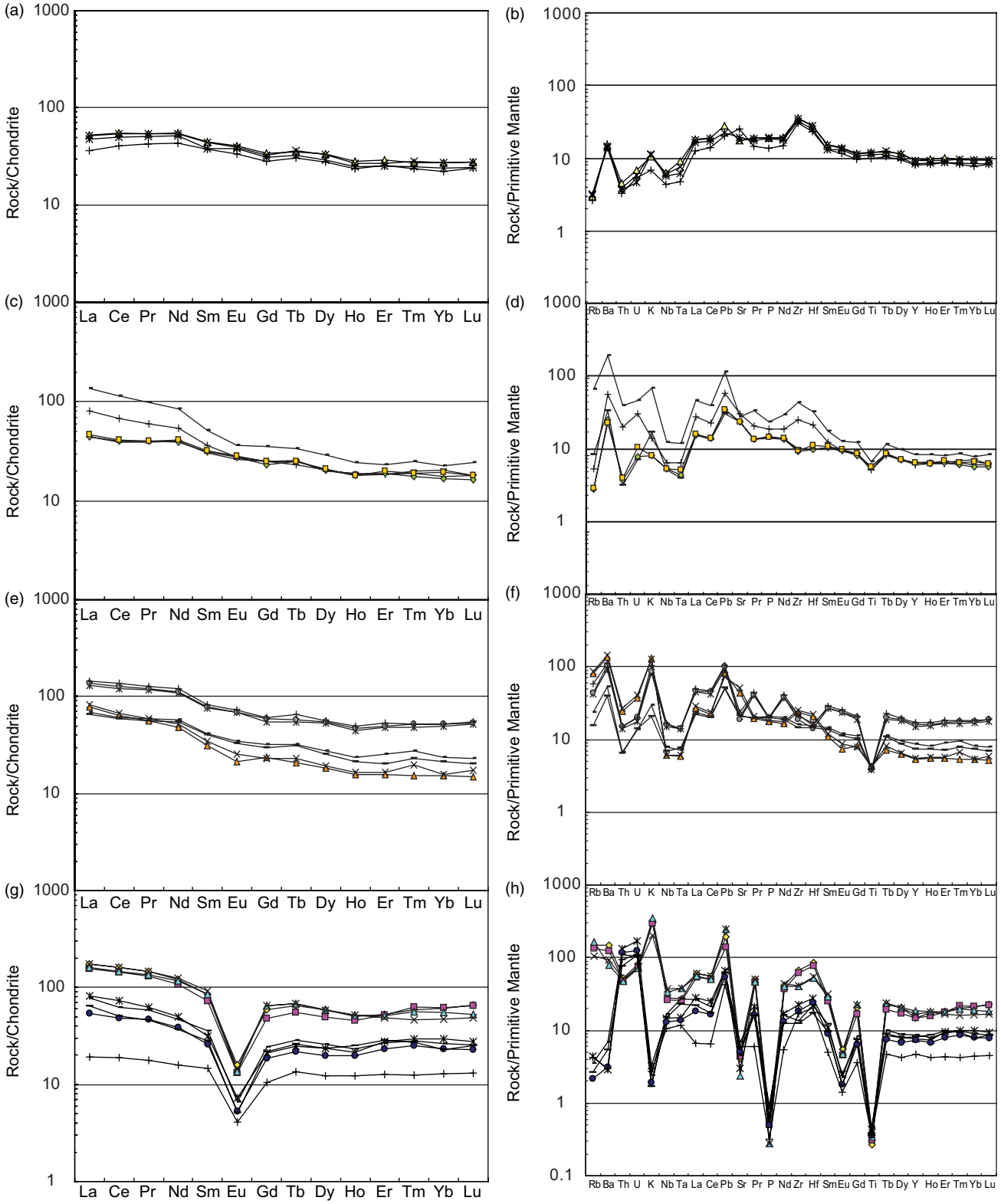

Fig. 8. Chondrite-normalized REE and primitive mantle (PM)-normalized multi-element diagrams for Permian volcanic rocks from the Kalatage area of the Turpan Basin. (a, b) Basalt samples, (c, d) basaltic andesite samples, (e, f) andesite samples, and (g, h) rhyolite samples from the Kalatage area of the Turpan Basin. Chondrite values are taken from Boynton (1984). The PM, N-MORB, E-MORB (enriched mid-ocean ridge basalt) and OIB (oceanic island basalt) values are taken from Sun & McDonough (1989).

https://doi.org/10.1017/S0016756819001006 Published online by Cambridge University Press

separation. All of these features and relations indicate that the volcanic rocks derived from the mantle, while their parent magmas may have undergone extensive levels of magmatic fractionation, during which intense interactions between residual melts and aqueous hydrothermal fluids occurred (likely rich in F and Cl).

The basalts, basaltic andesites and andesites show relatively high $\epsilon_{Nd}(t)$ levels, revealing that their parent magmas mainly originated from a depleted mantle. The sample presents $\epsilon_{Nd}(t)$ values of 4.6 to 8.2 and $(^{87}Sr/^{86}Sr)_i$ ratios of 0.70342 to 0.70591. The basalts present the highest $\epsilon_{Nd}(t)$ and lowest $(^{87}Sr/^{86}Sr)_i$ values, and the basaltic andesites present the lowest $\epsilon_{Nd}(t)$ values while rhyolites present the highest $(^{87}Sr/^{86}Sr)_i$ ratios. These variations in Sr and Nd isotopes observed between the different rocks suggest that their parent magmas were partly contaminated with arc-crustal components consistent with the Shaerhu complex (Mao *et al.* 2014) and with inherited zircon grains observed in the basaltic andesites.

In summary, the studied rhyolites are the product of the strong fractionation of depleted mantle-derived tholeiitic basic magma, which may serve as a mechanism of A-type granite genesis. The rocks originated from a depleted mantle and formed in a supra-subduction zone setting. These results are consistent with the fact that the Dananhu Arc was an island arc in the early Permian (Xiao *et al.* 2004, 2010; Windley *et al.* 2007).

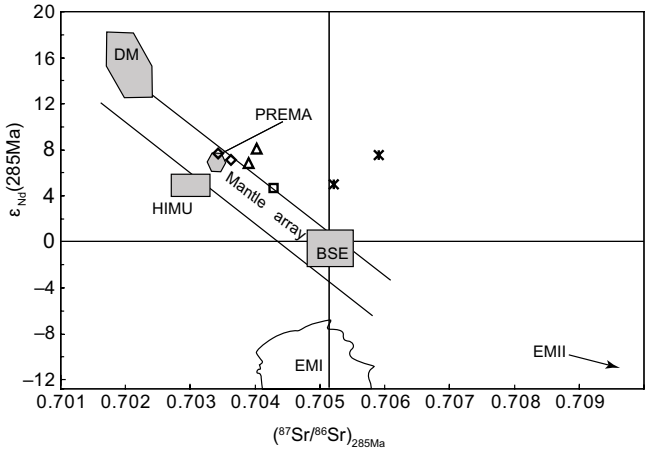

Fig. 9. $\epsilon_{Nd}(t)$ vs initial $(^{87}Sr/^{86}Sr)_i$ diagram for volcanic rocks from the Kalatage area of the Turpan Basin. DM, Depleted mantle; BSE, bulk silicate earth; EMI and EMII, enriched mantle; HIMU, mantle with high U/Pb ratio; PREMA, frequently observed mantle compositions (Zindler & Hart, 1986). Symbols used are the same as in Figure 6.

6.b. Accretionary tectonics of the southern Altaids

Our geochronology data indicate that the basaltic andesites and rhyolites may have erupted in 286.5 ± 2.1 Ma and 275.3 ± 1.8 Ma, respectively. Our results also reveal that the rhyolites erupted after the andesites in *c.* 10 Ma, and finally 10 Ma volcanism occurred in the Turpan Basin from 285 Ma to 275 Ma in the early Permian.

The early Permian is the key period for understanding the welding process occurring between the Tarim Block and southern active margins of the Palaeo-Asian Continent to the north (Ma *et al.* 1997; Li, 2004; Xiao *et al.* 2004, 2006, 2008*a*, *b*, 2010, 2013; Windley *et al.* 2007).

In the early Permian, large volumes of volcanic rocks and intrusions formed in NE Xinjiang, NW China (Fig. 1b; Table 4). For example, large volumes of mantle-derived basic–acidic volcanic rock formed in the Turpan Basin (Ma *et al.* 1997; Zhu *et al.* 2002; Zhou *et al.* 2006; Mao, 2014; Mao *et al.* 2014*c*), mantle-derived bimodal volcanism occurred from 296 Ma to 293 Ma in the southern Bogda and Haerlik Mountains (Zhou *et al.* 2006; Chen *et al.* 2011; Shu *et al.* 2011), and basalt formed rocks in the Santanghu Basin (Zhao *et al.* 2006*a*; Zhou *et al.* 2006; Wang, 2013). Early Permian alkali granitic intrusions occurred in the Balikun–Harlik, Bogda and Dananhu areas (Gu *et al.* 1999; Mao *et al.* 2008; Yuan *et al.* 2010; Zhou *et al.* 2010). Numerous Alaskan-type mafic–ultramafic intrusions of 269–285 Ma also occurred along large strike-slip shearing faults in the East Tianshan (Table 4; Han *et al.* 2004; Xiao *et al.* 2004, 2010; Zhou *et al.* 2004; JY Li *et al.* 2006*b*; Mao *et al.* 2006; Ao *et al.* 2010; Han *et al.* 2010; Qin *et al.* 2011). Finally, early Permian adakites of 274 Ma have been found in the Sanchakou and Huangshan areas (Li *et al.* 2004; Zhao *et al.* 2006*b*; Qin *et al.* 2009).

This form of magmatism is always connected to strike-slip tectonics occurring at the same time. For example, Laurent-Charvet *et al.* (2002, 2003) show that strike-slip shearing in the Chinese

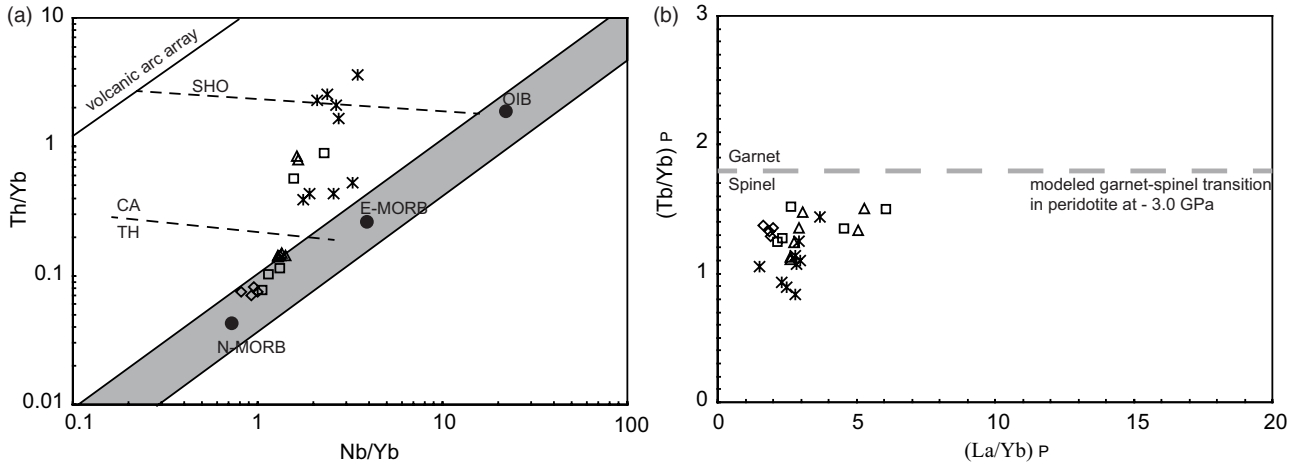

Fig. 10. (a) Th/Yb vs Nb/Yb diagram (Pearce, 1982, 2008) and (b) $(La/Yb)_P$ vs $(Sm/Yb)_P$ plot (modified after K Wang *et al.* 2002) for volcanic rocks from the Kalatage area of the Turpan Basin. SHO – shoshonite; CA – calc-alkaline; TH – tholeiite. All Tb/Yb and Sm/Yb values are normalized to the primitive mantle (Sun & McDonough, 1989).

https://doi.org/10.1017/S0016756819001006 Published online by Cambridge University Press

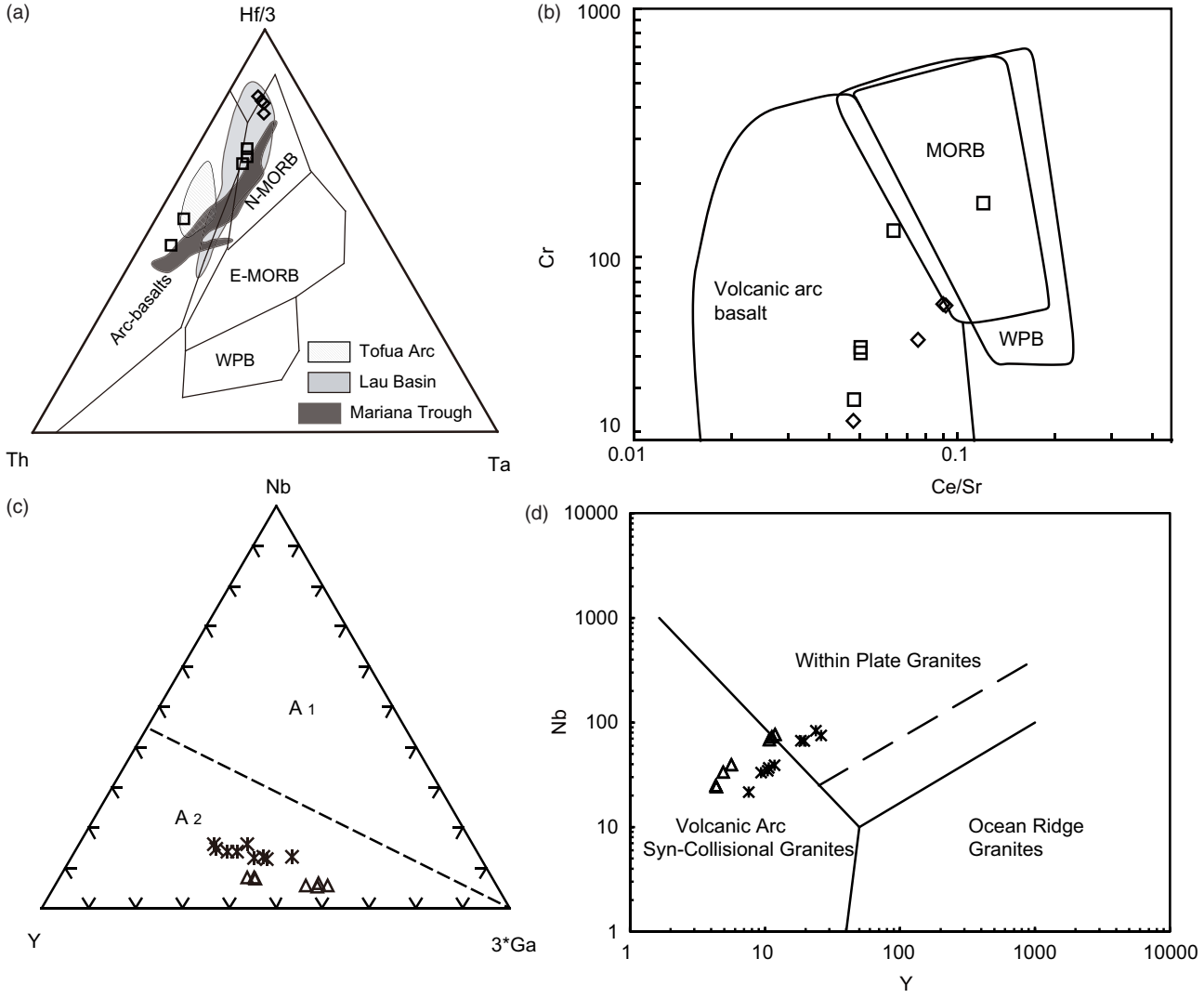

Fig. 11. (a) Zr–Zr/Y (Pearce & Norry, 1979) and (b) Hf–Th–Ta (Wood, 1980) discriminant diagrams for volcanic rocks (fields of the Tofua Arc, Lau Basin and Mariana Trough are taken from Hawkins (2003)); (c) Rb vs Y + Nb diagrams for volcanic rocks (Pearce *et al.* 1984); (d) Nb–Y–3Ga discriminant diagrams for the subdivision of A-type granites (Eby, 1992). Symbols used are the same as in Figure 6.

Tianshan and Altai mainly took place from 290 to 245 Ma. Other studies show that the ductile deformation of the Kangguer–Huangshan ductile zone formed from *c.* 260 to 247 Ma (Y Wang *et al.* 2002; YT Wang *et al.* 2004; W Chen *et al.* 2005) and/or from 267 to 275 Ma (Wang *et al.* 2014).

This form of mantle-derived magmatism, which occurs along extensional basins and strike-slip faults, has been widely reported and discussed (Allen *et al.* 1995, 1997; Xiao *et al.* 2004, 2010; Wang *et al.* 2009; Mao *et al.* 2014*c*). First, volcanic rocks occur along dextral strike-slip faults and related extensive basins, examples of which include the Shaerhu Complex within a NW-trending dextral strike-slip fault of the Dannanhu Arc of the early Permian (Chen *et al.* 2011; Mao, 2014; Mao *et al.* 2014*c*); basaltic rocks located along a NW-trending strike-slip fault within the Santanghu Basin (Zhao *et al.* 2006*a*); and extensional volcanic rocks positioned along NW-trending strike-slip faults of the Turpan Basin (illustrated in this work). In addition, Allen *et al.* (1995, 1997) have reported that the studied basins are connected to strike-slip faults of the region dating to the late Permian to Triassic. Second, many alkaline intrusions and mafic–ultramafic complexes intruded along regional faults of NE Xinjiang. For example, Dajiashan alkaline granites are exposed along the Kalameili fault (Mao *et al.* 2008), mafic–ultramafic intrusions developed in the Haibaotan Area (JY Li *et al.* 2006*b*), the Kalatongke mafic–ultramafic complex is positioned in the Erqis fault zone (Han *et al.* 2004), and Huangshan mafic–ultramafic belts are positioned in the Kangguer–Huangshan ductile zone (Xiao *et al.* 2004; Qin *et al.* 2011). Third, many syn-kinematic intrusions formed along major shear zones of the Tianshan Belt (e.g. in the Kangguer shear zones) (Wang *et al.* 2009, 2014; Branquet *et al.* 2012). In summary, early Permian subduction-related magmatism was correlated both in space and time with Permian strike-slip faults and extensional structures. This geological phenomenon has been widely studied and discussed. To date, a number of geological models have been proposed, most notably the mantle plume model (Pirajno *et al.* 2008; Qin *et al.* 2011; Su *et al.* 2012; Tang *et al.* 2013), the oblique subduction and oblique collision model (Mao *et al.* 2006; 2014*c*; Ao *et al.* 2010; Xiao *et al.* 2010), the post-collisional transtensional model (Allen *et al.* 1995, 1997; Wang *et al.* 2009, 2014; Branquet *et al.* 2012), the

https://doi.org/10.1017/S0016756819001006 Published online by Cambridge University Press

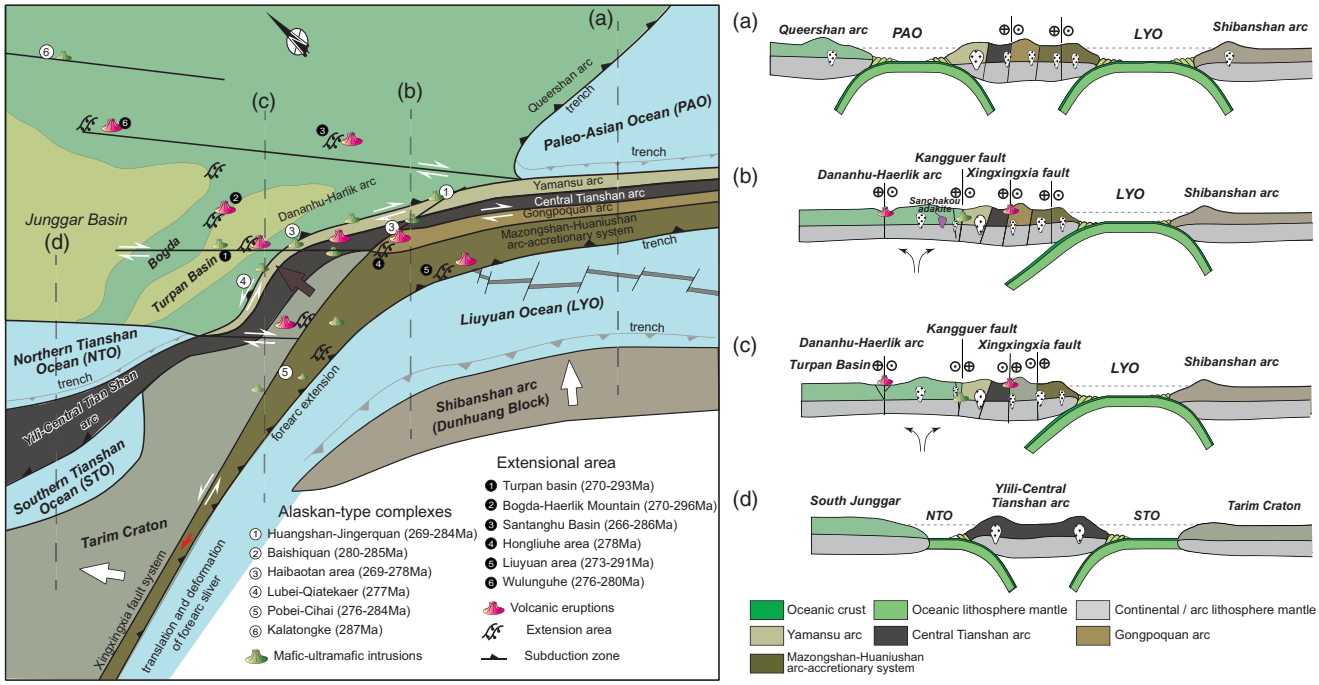

Fig. 12. Schematic tectonic diagrams illustrating the development of Permian volcanic rocks and intrusions in the East Tianshan (modified after Xiao *et al.* 2010; Mao *et al.* 2014*c*). (a) Tectonic cross-section of the Queershan Arc, Mazongshan–Huaniushan Arc accretionary system and Shibanshan Arc; (b) tectonic cross-section of the eastern part of the Kanggur shear zone and Dananhu–Haerlik Arc; (c) tectonic cross-section of the western part of the Kanggur shear zone, Dananhu–Haerlik Arc and Turpan Basin; (d) tectonic cross-section of the Yili – Central Tienshan Arc, Tarim Craton and Junggar Basin.

post-collisional slab break-off model (Yuan *et al.* 2010; Song *et al.* 2011; Deng *et al.* 2015; Du *et al.* 2018) and the post-collisional extension model (Han *et al.* 1997; Mao *et al.* 2002; Zhu *et al.* 2002; Zhou *et al.* 2004; JY Li *et al.* 2006*b*; Wang *et al.* 2006; Zhao *et al.* 2006*a*; Chen *et al.* 2011). Combining all of the data, it can therefore be considered to represent an oblique subduction of the Palaeo-Asian Ocean north of the Tarim Block (Ao *et al.* 2010; Xiao *et al.* 2010; Mao *et al.* 2014*c*), which may lead to transtension, tectonic extrusion and plate tearing in the East Tianshan. We conclude that early Permian magmatism was mantle-derived and formed in a forearc transtensional setting.

From the above data, other arguments and regional geological data, we propose a new tectonic scenario illustrated in Figure 12 that explains the emplacement of magmas along fault zones of different directions.

As demonstrated by Xiao *et al.* (2010) and Mao *et al.* (2014*c*), the Palaeo-Asian Ocean and Tarim Block were obliquely subducted to the southern active margins of the Palaeo-Asian continent (Xiao *et al.* 2008*b*, 2010; Mao *et al.* 2014*c*), which predictably led to the formation of extrusion tectonic, slab break-off (Tang *et al.* 2011), strike-slip faults and to transtension in the forearc of the East Tianshan (Chen *et al.* 2011; Mao *et al.* 2014*c*).

Forearc transtension may have occurred as a result of oblique subduction in the East Tianshan, possibly with slab break-off processes (Tang *et al.* 2011). The depleted mantle rose along the faults and spurred partial decompression melting to form volcanic rocks and intrusions along regional faults. The associated strike-slip faults cut the continental and/or arc blocks, carrying various forearc slices extruded outward (Chen *et al.* 2011; Mao *et al.* 2014*c*).

The described transtensional events were characterized by strike-slip faults and extensional basin formation, by the upwelling of magmas into the faults, and by the emplacement of intrusive and eruptive rocks into these basins and along deep strike-slip faults, e.g. large volumes of volcanic rocks and intrusions in the Turpan, Santanghu, Hongliuhe and Xiaoriquanzi basins and in the Haibotan–Kalatage, Kalatongke, Huangshan–Jingerquan, Lubei, Pobei–Cihai and Baishiquan mafic–ultramafic complexes (Table 4). Furthermore, N-MORB-like basalts erupted in a heavily extensional basin (e.g. the Turpan and Hongliuhe basins) (Fig. 12; Table 4). The described geological processes echo those of the Tanlu Fault in eastern China and those of the San Andreas Fault in North America. These strike-slip fault systems developed in the active continental margin, leading to the formation of continental extensions and mantle-derived magmas and even shaping the oceanic crust, e.g. the California Gulf. This system may echo the Jinsha River – Ailaoshan – Red River large strike-slip fault system extending through Yunnan Province from SW China to northern Vietnam and the Sagaing fault of SE Asia as well as large volumes of ultra-basic, basic, intermediate and felsic volcanic rocks formed along the Jinsha River – Ailaoshan – Red River strike-slip fault system of the late Oligocene to early Miocene (*c.* 27–22 Ma, Chung *et al.* 1997; Wang *et al.* 2001).

6.c. Implications for Palaeo-Pacific evolution

As noted above, interactions of the Palaeo-Pacific and Palaeo-Asian Oceans are an enigmatic issue due to their controversial temporal and spatial features, spurring contrasting views (either the Pacific Ocean only affected NE Asia in the Early Mesozoic, or the Palaeo-Pacific Ocean already operated in the Palaeozoic or even earlier (see Xiao *et al.* 2010, 2018)). The real cause of the observed divergence is the mutual translation of the Palaeo-Asian and Palaeo-Pacific Oceans in terms of temporal and spatial features.

The Palaeo-Asian Ocean constituted the main oceanic body, and its major branches extended from southern Mongolia to the

https://doi.org/10.1017/S0016756819001006 Published online by Cambridge University Press

north and from the Tarim and North China blocks to the south (Fig. 1). When the southern limb (southern Mongolia) of the Tuva Orocline rotated clockwise to collide with the Tarim and North China blocks, the Palaeo-Pacific Ocean closed. Therefore, the Palaeo-Asian Ocean formed part of the Palaeo-Pacific Ocean called the Panthalassic Ocean (Domeier & Torsvik, 2014; Xiao *et al.* 2015, 2018), and the timing of the closure of the Palaeo-Asian Ocean is key to developing a stronger understanding of the above-described process.

Located within the southernmost Altaids, the East Tianshan records the final phase of the closure of the Palaeo-Asian Ocean (Allen *et al.* 1993, 1995; Ma *et al.* 1997; Zhu *et al.* 2002; Laurent-Charvet *et al.* 2003; Xiao *et al.* 2004, 2010, 2015, 2018; Zhou *et al.* 2004; JY Li *et al.* 2006*b*; Mao *et al.* 2006, 2008, 2012, 2014*c*; JB Wang *et al.* 2006; Zhao *et al.* 2006*b*; B Wang *et al.* 2009, 2014; Ao *et al.* 2010; Yuan *et al.* 2010; Chen *et al.* 2011; Qin *et al.* 2011; Song *et al.* 2011; Branquet *et al.* 2012; Deng *et al.* 2015; Du *et al.* 2018). However, there has been no consensus on the closure of the Palaeo-Asian Ocean in the East Tianshan. Some researchers have argued that the closure of the Palaeo-Asian Ocean in the East Tianshan occurred in the Carboniferous (Allen *et al.* 1993, 1995; Laurent-Charvet *et al.* 2003; JB Wang *et al.* 2006; B Wang *et al.* 2009, 2014), while others have proposed a much later closure period occurring in the Permian or even in the Triassic (Xiao *et al.* 2004, 2015, 2018; Mao *et al.* 2006, 2014*c*; Ao *et al.* 2010; Domeier & Torsvik, 2014).

The former view is based on the fact that Devonian–Carboniferous tholeiitic basalts and calc-alkaline andesites in this region have been interpreted as island arc volcanic rocks (Ma *et al.* 1997; Rui *et al.* 2002; Song *et al.* 2002*a*; Xiao *et al.* 2004; Tang *et al.* 2006; Wan *et al.* 2006; Zhang *et al.* 2006; Wang *et al.* 2007). However, this verifies the fact that subduction occurred in the Carboniferous and does not serve as diagnostic evidence that subduction ended in the Carboniferous. The data presented in this paper provide solid evidence dating subduction processes later to the Permian. Therefore, the subduction of the Palaeo-Pacific Ocean may have been active in the Permian in the southern Altaids.

Acknowledgements. We appreciate Journal editors, Susie Bloor and Yildirim Dilek, the journal formal reviewer Yalcin Ersoy and an anonymous reviewer for their constructive comments that enhanced the presentation of the manuscript. This study was financially supported by the National Key Research and Development Program of China (2017YFC0601201), the National Natural Science Foundation of China (41888101), the Strategic Priority Research Program (B) of the Chinese Academy of Sciences (XDB18020203), the Chinese Geological Survey Project (DD20190815), the Chinese Ministry of Land and Resources for the Public Welfare Industry Research (201411026-1), the Chinese State 305 Project (2011BAB06B04-03) and the Key Research Program of Frontier Sciences, CAS (QYZDJ-SSW-SYS012). This is a contribution to IGCP 622.

References

Allen MB, Sengor AMC and Natalin B (1995) Junggar, Turfan and Alakol basins as late Permian to ? early Triassic extensional structures in a sinistral shear zone in the Altaid orogenic collage, central Asia. *Journal of the Geological Society* **152**, 327–38.

Allen MB and Vimcent SJ (1997) Fault reactivation in the Junggar region, northwest China: the role of basement structures during Mesozoic-Cenozoic compression. *Journal of the Geological Society* **154**, 151–5

Allen MB, Windley BF and Zhang C (1993) Palaeozoic collisional tectonics and magmatism of the Chinese Tienshan, central Asia. *Tectonophysics* **220**, 89–115.

Andersen T (2002) Correction of common lead in U-Pb analyses that do not report ^{204}Pb. *Chemical Geology* **192**, 59–79.

Ao SJ, Xiao WJ, Han CM, Mao QG and Zhang JE (2010) Geochronology and geochemistry of Early Permian mafic–ultramafic complexes in the Beishan area, Xinjiang, NW China: implications for late Paleozoic tectonic evolution of the southern Altaids. *Gondwana Research* **18**, 466–78.

Bazhenov ML, Collins AQ, Degtyarev KE, Levashova NM, Mikolaichuk AV, Pavlov VE and Voo RV (2003) Paleozoic northward drift of the North Tien Shan (Central Asia) as revealed by Ordovician and Carboniferous paleomagnetism. *Tectonophysics* **366**, 113–41.

Black LP, Kamo SL, Allen CM, Aleinkoff JN, Davis DW, Korsch RJ and Foudoulis C (2003) TEMORA 1: a new zircon standard for Phanerozoic U-Pb geochronology. *Chemical Geology* **200**, 155–70.

Bonin B, Grelou-Orsini C and Vialette Y (1978) Age, origin and evolution of the anorogenic complex of Evisa (Corsia): a K-Li-Sr study. *Contribution of Mineralogy and Petrology* **65**, 425–32.

Boynton WV (1984) Geochemistry of the rare earth elements: meteorite study. In *Rare Earth Element Geochemistry* (ed. P Henderson), pp. 63–114. Amsterdam: Elsevier.

Branquet Y, Guniaux C, Sizaret S, Barbanson L, Wang B, Cluzel D, Li GR and Delaunay A (2012) Synkinematic mafic/ultramafic sheeted intrusions: emplacement mechanism and strain restoration of the Permian Huangshan Ni–Cu ore belt (Eastern Tianshan, NW China), *Journal of Asian Earth Sciences* **56**, 240–57

Buchan C, Pfänder J, Kröner A, Brewer TS, Tomurtogoo O, Tomurhuu D, Cunningham D and Windley BF (2002) Timing of accretion and collisional deformation in the Central Asian orogenic belt: implications of granite geochronology in the Bayankhongor ophiolite zone. *Chemical Geology* **192**, 23–45.

Chao FG, Tu QJ, Zhang XM, Ren Y, Li GL and Dong FR (2006) Preliminary determination of the early Paleozoic magmatic arc in the Karlik Mountains, East Tianshan, Xinjiang, China: evidence from zircon SHRIMP U-Pb dating of granite bodies in the Tashuihe area. *Geological Bulletin of China* **25**, 923–7 (in Chinese with English abstract).

Chen F, Hagner E and Todt W (2000) Zircon ages And Nd isotopic and chemical compositions of orthogneisses from the Black Forest, Germany: evidence for a Cambrian magmatic arc. *International Journal of Earth Sciences* **88**, 791–802.

Chen FW, Li HQ, Chen YC, Wang DH, Wang JL, Liu DQ, Tang YL and Zhou RH (2005a) Zircon SHRIMP U-Pb dating and its geological significance of mineralization in Tuwu-Yandong porphyry copper mine, East Tianshan Mountain. *Acta Geologica Sinica* **79**, 256–61 (in Chinese with English abstract).

Chen W, Sun S, Zhang Y, Xiao WJ, Wang QL, Jiang LF and Yang JT (2005b) ^{40}Ar/^{39}Ar geochronology of the Qiugemingtashi-Huangshan ductile shear zone in East Tianshan, Xinjiang, NW China. *Acta Geologica Sinica* **79**, 790–804 (in Chinese with English abstract).

Chen XJ, Shu LS and Santosh IM (2011) Late Paleozoic post-collisional magmatism in the Eastern Tianshan Belt, Northwest China: new insights from geochemistry, geochronology and petrology of bimodal volcanic rocks. *Lithos* **127**, 581–98.

Chen ZH, Wang DH, Gong YF, Chen YC and Chen SP (2006) ^{40}Ar-^{39}Ar isotope dating of muscovite from Jingerquan pegmatite rare metal deposit in Hmni, Xinjiang, and its geological significance. *Mineral Deposits* **25**, 470–6 (in Chinese with English abstract).

Chung SL, Lee TY, Lo CH, Wang PL and Genyao W (1997) Intraplate extension prior to continental extrusion along the Ailao Shan-Red River shear zone. *Geology* **25**, 311–14.

Coleman RG (1989) Continental growth of Northwest China. *Tectonics* **8**, 521–635.

Condie KC (1989) Geochemical changes in Baslts and Andesites across the Archean–Proterozoic boundary: identification and significance *Lithos* **23**, 1–18.

Condie KC (2005) TTGs and adakites: are they both slab melts? *Lithos* **80**, 33–44.

Deng YF, Song XY, Hollings P, Zhou T, Yuan F, Chen LM and Zhang D (2015) Role of asthenosphere and lithosphere in the genesis of the

https://doi.org/10.1017/S0016756819001006 Published online by Cambridge University Press

early Permian Huangshan mafic–ultramafic intrusion in the northern Tianshan, NW China. *Lithos* **227**, 241–54.

Dobretsov NL, Berzin NA and Buslov MM (1995) Opening and the tectonic evolution of Paleo-Asian ocean. *International Geology Review* **35**, 335–60.

Domeier M and Torsvik TH (2014) Plate tectonics in the late Paleozoic. *Geoscience Frontiers* **5**, 303–50.

Du L, Long XP, Yuan C, Zhang YY, Huang ZY, Sun M and Xiao WJ (2018) Petrogenesis of Late Paleozoic diorites and A-type granites in the central Eastern Tianshan, NW China: response to post-collisional extension triggered by slab breakoff. *Lithos* **318–319**, 47–59.

Eby GN (1992) Chemical subdivision of the A-type granitoids: petrogenetic and tectonic implications. *Geology* **20**, 641–4.

Gao J, Li MS, Xiao XC, Tang YQ and He GQ (1998) Paleozoic tectonic evolution of the Tianshan orogen, northwestern China. *Tectonophysics* **287**, 213–31.

Gu LX, Hu SX, Chu Q, Yu CS and Xiao XJ (1999) Pre-collision granites and post-collision intrusive assemblage of the Kelameili-Harlik orogenic belt. *Acta Geologica Sinica* **73**, 316–29.

Gu LX, Yang H, Tao XC, Yan ZF, Li HM, Wang JD and Liu YD (1990) Rb-Sr geochronology of granites in the east section of the mid-Tianshan belt and its tectonic evolution. *Journal of Guilin College of Geology* **10**, 49–55 (inChinese with English abstract).

Guo HC, Zhong L and Li LQ (2006) Zircon SHRIMP U-Pb dating of quartz diorite in the Koumenzi area, Karlik Mountains, East Tianshan, Xinjiang, China, and its geological significance. *Geological Bulletin of China* **25**, 928–31 (in Chinese with English abstract).

Guo ZJ, Han BF, Zhang ZC, Deng ST and Liu C (2007) The discovery of Paleozoic leucogranite in eastern segment of Chinese middle Tianshan and its tectonic implications. *Acta Petrologica Sinica,* **23**, 1841–6.

Han B, Wang S, Jahn B-M, Hong D, Kagami H and Sun Y (1997) Depleted mantle source for the Ulungur River A-type granites from North Xinjiang, China: geochemistry and Nd-Sr isotopic evidence, and implications for the Phanerozoic crustal growth. *Chemical Geology* **138**, 135–59.

Han BF, He GQ, Wang SG and Hang DW (1998) Post-collisional mantle-derived magmatism and vertical growth of the continental crust in north Xinjiang. *Geological Review* **44**, 396–406 (in Chinese with English abstract).

Han BF, Song B, Chen LH and Li ZH (2004) Zircon U-Pb SHRIMP ages of the mafic-ultramafic complexes from the Halatongke and Huangshandong Cu–Ni sulfide deposits, in Xinjiang, and their tectonic significance. *Chinese Science Bulletin* **49**, 2324–8 (in Chinese).

Han CM, Xiao WJ, Zhao GC, Ao SJ, Zhang JE, Qu WJ and Du AD (2010) In-situ U-Pb, Hf and Re-Os isotopic analyses of the Xiangshan Ni-Cu-Co deposit in Eastern Tianshan (Xinjiang), Central Asia Orogenic Belt: constraints on the timing and genesis of the mineralization. *Lithos* **120**, 547–62.

Hawkins JW (2003) Geology of supra-subduction zones: implications for the origin of ophiolites. In *Ophiolite Concept and the Evolution of Geological Thought* (eds. Y Dilek and S Newcomb), pp. 227–68. Boulder, CO: Geological Society of America Special Paper 373.

Hollings P, Frakuck P and Kissin S (2004) Geochemistry and geodynamic implications of the Mesoproterozoic English Bay granite-rhyolite complex, northwest Ontario. *Canadian Journal of Earth Sciences* **41**, 1329–38.

Hou GS, Tang HF, Liu CQ and Wang YB (2005) Geochronological and geochemical study on the wallrock of Tuwu-Yandong porphyry copper deposits, eastern Tianshan mountains. *Acta Petrologica Sinica* **21**, 1729–36 (in Chinese with English abstract).

Hu AQ, Wei GJ, Deng WF, Zhang JB and Chen LL (2006) 1.4Ga SHRIMP U-Pb age for zircons of granodiorite and its geological significance from the eastern segment of the Tianshan Mountains, Xinjiang, China. *Geochimica* **35**, 333–45.

Hu AQ, Wei GJ, Jahn B, Zhang JB, Deng WF and Chen LL (2010) Formation of the 0.9Ga Neoproterozoic granitoids in the Tianshan Orogen, NW China: constraints from the SHRIMP zircon age determination and its tectonic significance. *Geochimica* **39**, 197–212.

Hu AQ, Wei GJ, Zhang JB, Deng WF and Chen LL (2007) SHRIMP U-Pb age for zircons of East Tianhu granitic gneiss and tectonic evolution significance from the eastern Tianshan Mountains, Xinjiang, China. *Acta Petrologica Sinica* **23**, 1795–802.

Irvine TN and Baragar WRA (1971) A guide to the chemical classification of the common volcanic rocks. *Canada Journal of Earth Science* **8**, 523–48.

Jahn BM (2004) The Central Asian Orogenic Belt and growth of the continental crust in the Phanerozoic. In *Aspects of the Tectonic Evolution of China* (eds J Malpas, CJN Fletcher, JC Aitchison & J Ali), pp. 73–100. Geological Society of London, Special Publication no. 226.

Jahn B-M, Wu F, Capdevila R, Martineau F, Zhao Z and Wang Y (2001) Highly evolved juvenile granites with tetrad REE patterns: the Woduhe and Baerzhe granites from the Great Xing'an Mountains in NE China. *Lithos* **59**, 171–98.

Jahn B-M, Wu F-Y and Chen B (2000) Granitoids of the Central Asian Orogenic Belt and continental growth in the Phanerozoic. *Transactions of the Royal Society of Edinburgh: Earth Sciences* **91**, 181–93.

Ji JS, Tao HX and Yang XK (1994) Geochemical characteristics of volcanic rocks within different tectonic settings in the central part of east Tianshan Mountains. *Acta Petrologica et Mineralogica* **13**, 297–304 (in Chinese with English abstract).

Johnson CL, Amory JA, Zinniker D, Lamb MA, Graham SA, Affolter M and Badarch G (2008) Sedimentary response to arc-continent collision, Permian, southern Mongolia. In *Formation and Applications of the Sedimentary Record in the Arc Collision Zones* (eds AE Draut, PD Clift and DW School), pp.363–90. Boulder, CO: Geological Society of America Special Paper 436.

Johnston ST, Weil AB and Gutierrez-Alonso G (2013) Oroclines: thick and thin. *Bulletin of the Geological Society of America* **125**, 643–63.

Laurent-Charvet S, Shu LS, Ma RS and Lu HF (2002). Palaeozoic late collisional strike-slip deformations in Tianshan and Altay, eastern Xinjiang, NW China. *Terra Nova* **14**, 249–56.

Laurent-Charvet S, Monie P, Charvet J and Shu L (2003) Late-Paleozoic strike-slip shear zones in northeastern Xinjiang (NW China): new structural and geochronological data. *Tectonics* **22**, 1009–32.

Le Maitre RW, Bateman P, Dudek A, Keller J, Lameyre LE, Bas MJ, Sabine PA, Schmid R, Sorensen H, Streckeisen A, Woolley AR and Zanettin B (1989) *A Classification of Igneous Rocks and Glossary of Terms*. Oxford: Blackwell.

Li D, He DF, Fan C, Xiang K and Jin LY (2013) Early Permian post-collisional magmatic events, East Junggar: constraints from zircon SHRIMP U-Pb age, geochemistry and Hf isotope of rhyolite in the Yundukala area. *Acta Petrologica Sinica* **29**, 317–37 (in Chinese with English abstract).

Li HQ, Chen FW, Lu YF, Yang HM, Guo J and Mei YP (2004) Zircon SHRIMP U-Pb age and strontium isotopes of mineralized granitoids in the Sanchakou copper polymetallic deposit, East Tianshan Mountains. *Acta Geoscentica Sinica* **25**, 191–5.

Li HQ, Chen FW, Mei YP, Wu H, Cheng SL, Yang JQ and Dai YC (2006) Isotopic ages of No. 1 intrusive body in Pobei mafic–ultramafic belt of Xinjiang and their geological significance. *Mineral Deposits* **25**, 463–9 (in Chinese with English abstract).

Li JY (2004) Late Neoproterozoic and Paleozoic tectonic framework and evolution of eastern Xinjiang, NW China. *Geological Review* **50**, 304–22 (in Chinese).

Li JY, He GQ, Xu X, Li HQ, Sun GH, Yang TN, Gao LM and Zhu ZX (2006a) Crustal tectonic framework of northern Xinjiang and adjacent and its formation. *Acta Geologica Sinica* **80**, 149–68 (in Chinese with English abstract).

Li JY, Song B, Wang KZ, Li YP, Sun GH and Qi DY (2006b) Permian mafic–ultramafic complexes on the southern margin of the Tu-Ha basin, eastern Tianshan Mountians: geological records of vertical crustal growth in central Asia. *Acta Geoscientica Sinica* **27**, 424–46 (in Chinese with English abstract).

Li QG, Liu SW, Song B, Wang YB and Chen Y (2009) Late Mesoproterozoic to Paleozoic tectonothermal events in the Eastern Segment of the Central Tianshan Tectonic Zone of Northwestern China: constraints from SHRIMP zircon geochronology. *Earth Science Frontiers* **16**, 175–84.

Li WP, Wang T, Li JB, Kang X, Yu FS, Han QJ and Ma ZP (2001) The U-Pb age of zircon from late Caledonian granitoid in Hongliuhe area, east Tianshan Mountains, Northwest China and its geological implications. *Acta Geoscientia Sinica* **22**, 121–8 (in Chinese with English abstract).

Li WQ, Wang R, Wang H and Xia B (2006c) Geochemistry and petrogenesis of the Kalatag intrusion in the "Tuha window". *Geology in China* **33**, 559–65 (in Chinese with English abstract).

https://doi.org/10.1017/S0016756819001006 Published online by Cambridge University Press

Li YH, Yang XK, Wang QL, Cui DX, Ji LY and Hao M (2012) Redetermination of the volcanic eruption time and analysis of geochemical characteristics of volcanic rocks in eastern Maotoushan of Beishan area, Xinjiang. *Geology in China* **39**, 683–94 (in Chinese with English abstract)

Liu SW, Guo ZJ, Zhang ZC, Li QG and Zhen HF (2004) Nature of Precambrian metamorphic blocks in Eastern Segment of the Central Tianshan: constraints from geochronology and Nd isotopic geochemistry. *Science in China: Series D* **34**, 395–403.

Loiselle MC and Wones DR (1979) Characteristics and origin of anorogenic granites. *Geological Society of America, Abstracts with Programs* **11**, 468.

Ludwig KR (2001) *Users Manual for Isoplot/Ex rev. 2.49*. Berkeley, California: Berkeley Geochronology Center, Special Publication no. 1a, 56 pp.

Ma RS, Shu LS and Sun J (1997) *Tectonic Evolution and Metalogeny of Eastern Tianshan Mountains*. Beijing: Geological Publishing House.

Mao JW, Yang JM, Qu WJ, Du AD, Wang ZL and Han CM (2002) Re-Os dating of Cu–Ni sulfide ores from Huangshandong deposit in Xinjiang and its geodynamic significance. *Mineral Deposits* **21**, 323–30 (in Chinese with English abstract).

Mao QG (2014) *The geological, metallogenesis and metallogenic prognosis studies of the Kalatage copper polymetallic ore district in eastern Tianshan, NW China*. Postdoctoral dissertation, Beijing Institute of Geology for Mineral Resources, Beijing, China, 150 pp.

Mao QG, Fang TH, Wang JB, Wang SL and Wang N (2010) The geochronology studies of the early Paleozoic Honghai massive sulfide deposits and its geological significance Kalatage belt, in eastern Tianshan mountain, Xinjiang, northwest China. *Acta Petrologica Sinica* **26**, 3017–26 (in Chinese with English abstract).

Mao QG, Wang JB, Fang TH, Yu MJ, Zhu JJ, Fu WW and Huang XK (2015) Lead and sulfur isotope studies of sulfides from Honghai VMS deposit in Kalatage ore belt of Eastern Tianshan Mountains. *Mineral Deposits* **34**, 730–44.

Mao QG, Wang JB, Xiao WJ, Fang TH, Wang N and Yu MJ (2014a) The discovery of low-Carboniferous arc volcanic rocks and its tectonic significance at the Kalatage Area in the central Tianshan, Eastern Tianshan Mountains, Xinjiang, NW China. *Acta Geologica Sinica* **88**, 1790–9 (in Chinese with English abstract).

Mao QG, Wang JB, Xiao WJ, Fang TH, Yu MJ, Ao SJ and Zhang JE (2014b) Stratigraphic, U-Pb (Zircon) and geochemical constraints on magmas, mineralization and geological evolution of the Kalatage district, the central part of Dananhu arc in eastern Tianshan Mountains. *Acta Geologica Sinica* **88**, 885–6.

Mao QG, Xiao WJ, Fang TH, Windley BF, Sun M, Ao SJ, Zhang JE and Huang XK (2014c) Geochronology, geochemistry and petrogenesis of Early Permian alkaline magmatism in the Eastern Tianshan: implications for tectonics of the Southern Altaids. *Lithos* **190–191**, 37–51.

Mao QG, Xiao WJ, Han CM, Sun M, Yuan C, Yan Z, Li JL, Yong Y and Zhang JE (2006) Zircon U-Pb age and the geochemistry of the Baishiquan mafic–ultramafic complex in the eastern Tianshan, Xinjiang: constraints on the closure of the Paleo-Asian Ocean. *Acta Petrologica Sinica* **22**, 153–62 (in Chinese with English abstract).

Mao QG, Xiao WJ, Han CM, Yuan C and Sun M (2008) Late Paleozoic southward accretionary polarity of the eastern Junggar orogenic belt: insight from the Dajiashan and other A-type granites. *Acta Petrologica Sinica* **24**, 733–42 (in Chinese with English abstract).

Mao QG, Xiao WJ, Windley BF, Han CM, Qu JF, Sun M, Ao SJ, Zhang JE and Guo QQ (2012) The Liuyuan complex in the Beishan, NW China: a Carboniferous-Permian ophiolitic fore-arc sliver in the southern Altaids. *Geological Magazine* **149**, 483–506.

McKenzie DAN and O'Nions RK (1991) Partial melt distributions from inversion of rare earth element concentrations. *Journal of Petology* **32**, 1021–91.

Meng QP, Chai FM, Li Q, Zheng JH, Shao FZ, Geng XX and Han WQ (2014) Zircon U-Pb geochronology, Hf isotopes and the petrogenesis of mafic intrusions in the Cihai Fe (-Co) deposit, Xinjiang. *Acta Petrologica Sinica* **30**, 109–12 (in Chinese with English abstract).

Myashiro A (1974) Volcanic series in island arc and active continental margins. *American Journal of Science* **274**, 321–55.

Pan JH, Guo ZJ, Liu C and Zhao ZH (2008) Geochronology, geochemistry and tectonic implications of Permian basalts in Hongliuhe area on the border between Xinjinga and Gansu. *Acta Petrologica Sinica* **24**,793–802 (in Chinese with English abstract).

Pearce JA (1982) Trace element characteristics of lavas from destructive plate boundaries. In *Orogenic Andesites and Related Rocks* (ed. RS Thorpe), pp. 528–48. Chichester: John Willey & Sons.

Pearce JA (2008) Geochemical fingerprinting of oceanic basalts with applications to ophiolite classification and the search for Archean oceanic crust. *Lithos*, **100**, 14–48.

Pearce JA and Cann JR (1973) Tectonic setting of basic volcanic rocks determined using trace element anlyses. *Earth and Planetary Sciences Letters* **19**, 290–300.

Pearce JA, Harris NBW and Tindle AG (1984) Trace element discrimination diagrams for the tectonic interpretation of granitic rocks. *Journal of Petrology* **25**, 956–83.

Pearce JA and Norry MJ (1979) Petrogenetic implications of Ti, Zr, Y and Nb variations in volcanic rocks. *Contributions to Mineralogy and Petrology* **69**, 33–47.

Pirajno F, Mao JW, Zhang ZH, Chai FM (2008) The association of mafic–ultramafic intrusions and A-type magmatism in the Tian Shan and Altay orogens, NW China: implications for geodynamic evolution and potential for the discovery of new ore deposits. *Journal of Asian Earth Sciences* **32**, 165–83.

Qin KZ, Fang TH, Wang SL and Wang XD (2001) Discovery of the Kalatage Cu-Au mineralized district and its prospecting potentiality, in the Paleozoic uplift at the south margin of the Tu-Ha Basin. *Geology in China* **28**, 16–23 (in Chinese).

Qin KZ, Su BX, Sakyi PA, Tang DM, Li XH, Sun H, Xiao QH and Liu PP (2011) SIMS zircon U-Pb geochronology and Sr-Nd isotopes of Ni-Cu-bearing mafic-ultramafic intrusions in eastern Tianshan and Beishan in correlation with flood basalts in Tarim basin (NW China): constraints on a ca. 280 Ma mantle plume. *American Journal of Science* **311**, 237–60.

Qin KZ, Zhang LC, Ding KS, Xu YX, Tang DM, Xu XW, Ma TL and Li GM (2009) Mineralization type, petrogenesis of ore-bearing intrusions and mineralogical characteristics of Sanchakou copper deposits in eastern Tianshan, *Acta Perologica Sinica* **25**, 845–61 (in Chinese with English abstract).

Rui ZY, Wang LS and Wang YT (2002) Discussion on metallogenic epoch of Tuwu and Yandong porphyry copper deposits in eastern Tianshan Mountains, Xinjiang. *Mineral Deposits* **21**, 16–22 (in Chinese with English abstract).

Şengör AMC and Natal'in B (1996) Turkic-type orogeny and its role in the making of the continental crust. *Annual Reviews of Earth and Planetary Sciences* **24**, 263–337.

Şengör AMC, Natal'in BA and Burtman US (1993) Evolution of the Altaid tectonic collage and Paleozoic crustal growth in Eurasia. *Nature* **364**, 209–304.

Shi WX, Liao QA, Hu YQ and Yang ZH (2010) Characteristics of mesoproterozoic granites and their geological significances from middle Tianshan block, East Tianshan district, NW China. *Geological Science and Technology Information* **29**, 29–37 (in Chinese with English abstract).

Shu LS, Charvert J, Guo HF, Lu HX and Laurent-Charvet S (1999) A large-scale dextral ductile strike slip zone: the Aqqikkudug-Weiya zone along the northern margin of the Central Tianshan belt, Xingjiang, NW China. *Acta Geologica Sinica* **73**, 148–62.

Shu LS, Wang B, Zhu WB, Guo ZJ, Charvet J and Zhang Y (2011) Timing of initiation of extension in the Tianshan, based on structural, geochemical and geochronological analyses of bimodal volcanism and olistostrome in the Bogda Shan (NW China). *International Journal of Earth Sciences* **100**, 1647–63.

Song B, Li JY, Li WP, Wang KZ and Wang YB (2002a) SHRIMP dating of the Dananhu and Kezirkalasayi granitoids batholiths in southern margin of Tuha Basin and their geological implication. *Xingjiang Geology* **20**, 332–45 (in Chinese with English abstract).

Song B, Zhang YH, Wan YS and Jian P (2002b) Mount Making and procedure of the SHRIMP dating. *Geological Review* **48**, 26–30 (Suppl., in Chinese).

Song XY, Xie W, Deng YF, Crawford AJ, Zheng WQ, Zhou GF, Deng G, Cheng SL and Li J (2011) Slab break-off and the formation of Permian

https://doi.org/10.1017/S0016756819001006 Published online by Cambridge University Press

mafic–ultramafic intrusions in southern margin of central Asian orogenic belt, Xinxiang, NW China. *Lithos* **127**, 128–43.

Su BX, Qin KZ, Sun H, Tang DM, Sakyi PA, Chu ZY, Liu PP, Xiao QH (2012) Subduction-induced mantle heterogeneity beneath Eastern Tianshan and Beishan: insights from Nd-Sr-Hf-O isotopic mapping of Late Paleozoic mafic–ultramafic complexes. *Lithos*, **134–135**, 41–51.

Sun GH, Li JY, Gao LM and Yang TN (2005) Zircon SHRIMP U-Pb age of a dioritic pluton in the Harlik mountain, eastern Xinjiang, and its tectonic implication. *Geological Review* **51**, 463–9 (in Chinese with English abstract).

Sun GH, Li JY, Wang DG, Gao LM and Song AJ (2006) Zircon SHRIMP U-Pb ages of granite and granodiorite at the south side of the Aqikkuduk fault, east Tianshan, Xinjiang, China, and its tectonic implications. *Geological Bulletin of China* **25**, 945–52.

Sun SS and McDonough WF (1989) Chemical and isotopic systematic of oceanic basalts: implicattions for mantle composition and process, In *Magmatism in the Ocean Basins* (eds. AD Sauders and MJ Norry), pp. 313–45. Geological Society of London, Special Publication no. 42.

Sun T, Qian ZZ, Tang ZL, Jiang CY, He K, Sun YL, Wang JZ and Xia MZ (2010) Zircon U-Pb chronology, platinum group element geochemistry characteristics of Hulu Cu–Ni deposit East Xinjiang, and its geological significance. *Acta Petrologica Sinica*, **26**, 3339–49 (in Chinese with English abstract).

Tang DM, Qin KZ, Su BX, Sakyi PA, Liu YS, Mao Q, Santosh M and Ma YG (2013) Magma source and tectonics of the Xiangshanzhong mafic–ultramafic intrusion in the Central Asian Orogenic Belt, NW China, traced from geochemical and isotopic signatures. *Lithos* **170–171**, 144–63.

Tang HJ, Meng GX, Yang YQ, Deng Z, Yan JY, Qi G and Xue RH (2018) Geological and Geochemical features of the Permian bimodal volcanic rocks in the Qiakurtu Area, Eastern Junggar Basin, Xinjiang. *Geological Review* **64**, 1393–412 (in Chinese with English abstract).

Tang JH, Gu LX, Zheng YC, Fang TH, Zhang ZZ, Gao JH, Wang FT, Wang CS and Zhang GH (2006) Petrology,geochemistry and genesis of the Na-rich volcanic rocks of the Kalatag area, eastern Tianshan. *Acta Petrologica Sinica* **22**, 1150–66 (in Chinese with English abstract).

Tang DM, Qin KZ, Li CS, Qi L, Su BX and Qu WJ (2011) Zircon dating, Hf–Sr–Nd–Os isotopes and PGE geochemistry of the Tianyu sulfide-bearing mafic–ultramafic intrusion in the Central Asian Orogenic Belt, NW China. *Lithos* **126**, 84–98.

Turner SP, Foden JD and Morrison RS (1992) Derivation of some A-type magmas by fractionation of basaltic magma; an example from the Padthaway Ridge, South Australia. *Lithos* **28**, 151–79.

Wan B, Zhang LC, Xu XW and Sun H (2006) Geochemical characteristics of volcanic, sub-volcanic rocks in Xiaoshitouquan copper polymetallic deposit, eastern Tianshan, and its metallogenic setting. *Acta Petrologica Sinica* **22**, 2711–18 (in Chinese with English abstract).

Wang B, Cluzel D, Jajn BM, Shu L, Chen Y, Zhai Y, Branquet Y, Barbanson L and Sizaret S (2014) Late Paleozoic pre- and syn-kinematic plutons of the Kangguer-Huangshan shear zone: inference on the tectonic evolution of the eastern Chinese north Tianshan. *American Journal of Science* **314**, 43–79.

Wang B, Cluzel D, Shu L, Faure M, Charvet J, Chen Y, Meddre S and Jong K (2009) Evolution of calc-alkaline to alkaline magmatism through carboniferous convergence to Permian transcurrent tectonics, western Chinese Tianshan. *International Journal of Earth Sciences* **98**, 1275–98.

Wang JB, Wang YW and He ZJ (2006) Ore deposits as a guide to the tectonic evolution in the East Tianshan Mountains, NW China. *Geology in China* **33**, 461–9 (in Chinese with English abstract).

Wang JH, Yin A, Harrison TM, Grove M, Zhang YQ and Xie GH (2001) A tectonic model for Cenozoic igneous activities in the eastern Indo-Asian collision zone. *Earth and Planetary Science Letters*, **188**, 123–33.

Wang K, Plank T, Walker JD and Smith EI (2002) A mantle melting profile across the Basin and Range, SW USA. *Journal of Geophysical Research* **107**, B1. doi: 10.1029/2001JB000209.

Wang Q, Wyman DA, Zhao ZH, Xu JF, Zheng HB, Xiong XL, Dai DX, Li HC and Chu ZY (2007) Petrogenesis of Carboniferous adakites and Nb-enriched arc basalts in the Alataw area, northern Tianshan range (western China): implications for Phanerozoic crustal growth in the central Asia orogenic belt. *Chemical Geology* **236**, 42–64.

Wang SS (2013) *Mid-Permian magmatic activities and dynamic background for basin forming in Santanghu Area of Xinjiang*. Postdoctoral dissertation, Northwest University, China, 146 pp (in Chinese with English abstract).

Wang Y, Li JY and Li WQ (2002) $^{40}Ar/^{39}Ar$ chronological evidence of dextral shear and tectonic evolution of the Eastern Tianshan Orogenic Belt. *Xinjiang Geology* **20**, 315–19 (in Chinese with English abstract).

Wang YL, Zhang ZW, You MX, Li X, Li K and Wang BL (2015) Chronological and geochemical characteristics of the Baixintan Ni-Cu deposit in Eastern Tianshan Mountains, Xinjiang, and their implications for Ni-Cu mineralization. *Geology in China* **42**, 452–67 (in Chinese with English abstract).

Wang YT, Mao JW, Li XF and Yang FQ (2004) Gold metallization related to shear zone. *Earth Science Frontiers* **11**, 393–400 (in Chinese with English abstract).

Whalen JB, Currie KL and Chappell BW (1987) A-type granites: geochemical characteristics, discrimination and petrogenesis. *Contribution to Mineralogy and Petrology* **95**, 407–19.

Wilson M (1989) *Igneous Petrogenesis: A Global Tectonic Approach*. London: Unwin Hyman, pp. 101–50.

Wilson M (2001) *Igneous Petrogenesis: A Global Tectonic Approach*. Dordrecht: Kluwer Academic Publishers, pp. 245–85.

Windley BF, Alexeiev D, Xiao W, Kröner A and Badarch G (2007) Tectonic models for accretion of the Central Asian Orogenic belt. *Journal of the Geological Society, London* **164**, 31–47.

Windley BF, Allen MB, Zhang C, Zhao ZY and Wang GR (1990) Paleozoic accretion and Cenozoic redeformation of the Chinese Tien Shan Range, Central Asia. *Geology* **18**, 128–31.

Wood DA (1980) The application of a Th-Hf-Ta diagram to problems of tectonomagmatic classification and to establishing the nature of crustal contamination of basaltic lavas of the British Tertiary volcanic province. *Earth and Planetary Science Letters* **50**, 11–30.

Wu FY, Jahn BM, Wilde SA and Sun DY (2000) Phanerozoic crustal growth: U-Pb and Sr-Nd isotopic evidence from the granites in northeastern China. *Tectonophysics* **328**, 89–113.

Wu FY, Sun DY, Li HM, Jahn BM and Wilde SA (2002) A-type granites in northeastern China: age and geochemical constraints on their petrogenesis. *Chemical Geology* **187**, 143–73.

Wu H, Li HQ, Mo XH, Chen FW, Lu YF, Mei YP and Deng G (2005) Age of the Baishiqun mafic–ultramafic complex, Hami, Xinjiang and its geological significance. *Acta Geologica Sinica* **79**, 498–502 (in Chinese with English abstract).

XBGMR (Xinjiang Bureau of Geology and Mineral Resources) (1993) *Regional Geology of Xinjiang Autonomous Region, Geological Memoirs, Ser. 1, No. 32, Map Scale 1: 1,500,000*. Beijing: Geological Publishing House.

Xiao W, Windley B, Sun S, Li J, Huang B, Han C, Yuan C, Sun M & Chen H (2015) A tale of amalgamation of three collage systems in the Permian-Middle Triassic in Central Asia: oroclines, sutures and terminal accretion. *Annual Review of Earth and Planetary Sciences* **43**, 477–507. doi: 10.1146/annurev-earth-060614-105254.

Xiao W, Windley BF, Han C, Liu W, Wan B, Zhang JE, Ao S, Zhang Z and Song D (2018) Late Paleozoic to early Triassic multiple roll-back and oroclinal bending of the Mongolia collage in Central Asia. *Earth-Science Reviews* **186**, 94–128.

Xiao WJ, Han CM, Yuan C, Chen HL, Sun M, Lin SF, Li ZL, Mao QG, Zhang JE, Sun S and Li JL (2006) The unique Carboniferous-Permian tectonic-metallogenic framework of Northern Xinjiang (NW China): constraints for the tectonics of the southern Paleoasian Domain. *Acta Petrologica Sinica* **22**, 1362–76 (in Chinese with English abstract).

Xiao WJ, Han CM, Yuan C, Sun M, Lin SF, Chen HL, Li ZL, Li JL and Sun S (2008a). Middle Cambrian to Permian subduction-related accretionary orogenesis of North Xinjiang, NW China: implications for the tectonic evolution of Central Asia. *Journal of Asian Earth Sciences* **32**, 102–17. doi: 110.1016/j.jseas.2007.1010.1008.

Xiao WJ, Mao QG, Windley BF, Qu JF, Zhang JE, Ao SJ, Guo QQ, Cleven NR, Lin SF, Shan YH and Li JL (2010) Paleozoic multiple accretionary and collisional processes of the Beishan orogenic collage. *American Journal of Science* **310**, 1553–94.

https://doi.org/10.1017/S0016756819001006 Published online by Cambridge University Press

Xiao WJ, Shu LS, Gao J, Xiong XL, Wang JB, Guo ZJ, Li JY and Sun M (2008b) Continental dynamics of the Central Asian Orogenic Belt and its metallogeny. *Xinjiang Geology* **26**, 4–8.

Xiao WJ, Windley BF, Allen MB and Han CM (2013) Paleozoic multiple accretionary and collisional tectonics of the Chinese Tianshan orogenic collage. *Gondwana Research* **23**, 1316–41.

Xiao WJ, Zhang LC, Qin KZ, Sun S and Li JL (2004) Paleozoic accretionary and collisional tectonics of the Eastern Tianshan (China): implications for the continental growth of central Asia. *American Journal of Science* **304**, 370–95.

Xie LW, Zhang YB, Zhang HH, Sun JF and Wu FY (2008) In situ simultaneous determination of trace elements, U-Pb and Lu-Hf isotopes in zircon and baddeleyite. *Chinese Science Bulletin* **53**, 1565–73.

Xiu QY, Yu HF and Li Q 2002. A single zircon U-Pb age for the granodiorite of Kawabulark complex, Xinjiang, China. *Xinjiang Geology* **20**, 335–7.

Yakubchuk A (2004) Architecture and mineral deposit settings of the Altaid orogenic collage: a revised model. *Journal of Asian Earth Sciences* **23**, 761–79

Yang XK, Ji JS, Zhang LC and Zeng ZR (1998) Basic features and gold prognosis of the regional ductile shear zone in Eastern Tianshan. *Geotectonica et Metallogenia* **22**, 209–18 (in Chinese with English abstract).

Yang XK, Tao HX, Luo GC and Ji JS (1996) Basic features of plate tectonics in Eastern Tianhan of China. *Xinjiang Geology* **25**, 1901–15 (in Chinese with English abstract).

Yuan C, Sun M, Wilde S, Xiao WJ, Xu YG, Long XP and Zhao GC (2010) Postcollisional plutons in the Balikun area, East Chinese Tianshan: evolving magmatism in response to extension and slab break-off. *Lithos* **119**, 269–88.

Yuan C, Sun M, Xiao WJ, Li XH, Chen HL, Lin SF, Xia XP and Long XP (2007) Accretionary orogenesis of Chinese Altai: insights from the Paleozoic Granitoids. *Chemical Geology* **242**, 22–39.

Zhang LC, Wan B, Jiao XJ and Zhang R (2006) Characteristics and geological significance of adakitic rocks in copper-bearing porphyry in Baogutu, western Junggar. *Geology in China* **33**, 626–31 (in Chinese with English abstract).

Zhang YY, Dostal J, Zhao ZH, Liu C and Guo Z (2011) Geochronology, geochemistry and petrogenesis of mafic and ultramafic rocks from Southern Beishan area, NW China: implications for crust–mantle interaction. *Gondwana Research* **20**, 816–30.

Zhang ZZ, Gu LX, Yang H, Wu CZ, Wang YX and Min MZ (2004) Characteristics and genesis of the Chengjiangian gneissic granites in the east section of the Middle Tianshan Mountain areas: taking the Tianhudong granite as an example. *Acta Petrologica Sinica* **20**, 595–608 (in Chinese with English abstract).

Zhao Z, Masuda A and Shabani M (1992) REE tetrad effects in rare metal granite. *Chinese Journal of Geochemistry* **12**, 221–33.

Zhao ZH, Guo ZJ, Han BF and Wang Y (2006a) The geochemical characteristics and tectonic-magmatic implications of the latest-Paleozoic volcanic rocks from Santanghu basin, eastern Xinjiang, northwest China. *Acta Petrologica Sinica* **22**, 199–214 (in Chinese with English abstract).

Zhao ZH, Wang Q, Xiong XL, Zhang HX, Niu HC, Xu Jf, Bai ZH, Qiao YL (2006b) Two types of adakites in north Xinjiang, China. *Acta Petrologica Sinica* **22**, 1249–65 (in Chinese with English abstract).

Zhao ZH, Xiong XL, Han XD, Wang YX, Wang Q, Bao ZW and Jahn BM (2002) Controls on the REE tetrad effect in granites: evidence from the Qianlishan and Baerzhe Granites, China. *Geochemical Journal* **36**, 527–43.

Zhou DW, Liu YQ, Xing XJ, Hao JR, Dong YP and Ouyang ZJ (2006) The Permian Basalt magmatic activities and tectonic implication for the dynamic background of the Santanghu and Turpan basin, Xinjiang. *Science in China Series D Earth Sciences* **36**, 143–53 (in Chinese).

Zhou M-F, Lesher CM, Yang ZX, Li JW and Sun M (2004) Geochemistry and petrogenesis of 270 Ma Ni-Cu- (PGE) sulfide-bearing mafic intrusions in the Huangshan district, Eastern Xinjiang, Northwest China: implications for the tectonic evolution of the Central Asian orogenic belt. *Chemical Geology* **209**, 233–57.

Zhou TF, Yuan F, Zhang DY, Fan Y, Liu S, Peng MX and Zhang JD (2010) Geochronology, tectonic setting and mineralization of granitoids in Jueluotage area, eastern Tianshan, Xinjiang. *Acta Petrologica Sinica* **26**, 478–502.

Zhou XH, Sun, M, Zhang GH and Chen SH (2002) Continental crust and lithospheric mantle interaction beneath North China: isotopic evidence from granulite xenoliths in Hannuoba, Sino-Korean craton. *Lithos* **62**, 111–24.

Zhu WB, Ma RS, Guo JC, Sun, Y. Guo LZ, Xu MJ and Hu DZ (2002) The coupling of sedimentary characteristics and tectonic development of Turpan-Hami basin and adjacent areas in Early Permian. *Geological Journal of China Universities* **8**, 160–8 (in Chinese with English abstract).

Zindler, A. & Hart SR (1986) Chemical geodynamics. *Annual Reviews of Earth and Planetary Sciences* **14**, 493–571.

https://doi.org/10.1017/S0016756819001006 Published online by Cambridge University Press